BRNO UNIVERSITY OF TECHNOLOGY
VYSOKÉ UČENÍ TECHNICKÉ V BRNĚ

FACULTY OF MECHANICAL ENGINEERING
FAKULTA STROJNÍHO INŽENÝRSTVÍ

INSTITUTE OF PHYSICAL ENGINEERING
ÚSTAV FYZIKÁLNÍHO INŽENÝRSTVÍ

OPTICAL STUDY OF LASER-INDUCED MAGNETIC PHASE TRANSITIONS
OPTICKÉ STUDIUM LASEREM INDUKOVANÝCH MAGNETICKÝCH FÁZOVÝCH PŘECHODŮ

BACHELOR'S THESIS
BAKALÁŘSKÁ PRÁCE

AUTHOR
AUTOR PRÁCE
ALEXANDER VELIČ

SUPERVISOR
VEDOUCÍ PRÁCE
M.Sc. JON ANDER ARREGI URIBEETXEBARRIA, Ph.D.

BRNO 2022

Abstract
Na vykonanie ultrarýchleho ukladania údajov na základe magnetických materiálov sa skúma nový spôsob sub-pikosekundovej magnetizácie. Železo-ródium sa navrhuje ako vhodný materiál, ktorý je schopný vykonávať laserom indukovanú magentizáciu. Prípravy na tento experiment pozostávajú z rastu vzorky pomocou metódy fyzikálneho naparovania magnetrónovým naprašovaním a následnej charakterizácie vzorky. Boli pripravené tri vzorky, každá s iným konceptom teplotného ladenia. Ukážka I je vyladená zmenou kompozície ($Fe_{1-x}Rh_x$). Uloženie vzorky II na zafírový substrát indukované ťahovým napätím v rovine. Dopovaním uhlíka železo-ródiového tenkého filmu vzorky III. Tenkovrstvové vzorky sú charakterizované použitím vibračnej magnetometrie vzorky a optickej mikroskopie. Vibračná magnetometria vzorky poskytla spôsob zaznamenávania hysteréznych kriviek riadených poľom a čo je dôležitejšie, aj tepelne. Merania poskytli presné hodnoty teplôt fázového prechodu pre antiferomagnetické-k-feromagnetické a feromagnetické antiferomagnetické vzorky I, II a III boli určené na 325,9 K a 306 K, 321 K a 291 K, respektíve 311,8 K a 288 K. Boli zaznamenané charakteristické hodnoty saturácie magnetizácie, koercitívneho poľa, pomer zvyškovej magnetizácie a teplotného rozdielu medzi teplotami fázového prechodu. Vlastný kód v kombinácii s mikroskopickými obrázkami ponúkal dômyselné informácie o raste domén špecifických pre povrchovú oblasť. Kombinácia výsledkov oboch metód umožnila hlbšie pochopenie ‘’ako’’ a ,‘‘kedy‘‘ vyššie uvedený magnetoštrukturálny fázový prechod. Ultrarýchla laserom indukovaná magnetizácia využíva vlastný dizajn lasera. Pozorovanie ožiareného tenkého filmu železoródia pomocou optickej mikroskopie ukazuje stabilné feromagnetické domény na vzorke v laserovej dráhe. Dospeli sme teda k záveru, že sú pripravené tenké vrstvy železo-ródia charakterizované magnetometriou ako funkcia teploty a bola úspešne vykonaná ultrarýchla magnetizácia indukovaná laserom.

Summary
To perform ultrafast storage of data based on magnetic materials, a new way of subpicosecond magnetization is researched. Iron-Rhodium is suggested as convenient material which is capable of performing laser induced magentization. Preparations for this experiment consists of sample growth using physical vapor deposition method of magnetron sputtering and subsequent sample characterization. Three samples were prepared, each with different concept of temperature tuning. Sample I is tuned via composition alteration ($Fe_{1-x}Rh_x$). Sample II deposition onto a sapphire substrate induced tensile in-plane stress. By carbon doping Iron-Rhodium thin film of sample III. The thin film samples are characterized by using vibrating sample magnetometry and optical microscopy. Vibrating sample magnetometry granted a way of recording field driven and more importantly thermally driven hysteresis curves. Measurements yielded precise values of phase transition temperatures for antiferromagnetic-to-ferromagnetic and ferromagnetic-to-antiferromagnetic were detetermined for samples I, II, and III to be 325.9 K and 306 K, 321 K and 291 K, and 311.8 K and 288 K, respectively. Characteristic values of magnetization saturation, coercive field, residual magnetization and temperature difference between phase transition temperatures were recorded. Custom code in combination with microscopy images offered an insightful information on surface region specific domain growth. Combining results of both methods granted a deeper understanding of "how" and "when" aforementioned magnetostructural phase transition takes affect. The ultrashort laser induced magnetization utilizes a custom laser set-up. The observation of irradiated

FeRh thin film using optical microscopy shows stable ferromagnetic domains in a laser path pattern. Thus concluding that FeRh thin films are prepared, characterized by magnetometry as a function of temperature, and the ultrafast laser induced magnetization was successfully performed.

Klíčová slova
Ukladanie dát, Fe-Rh, magnetoštrukturálny fázový prechod, laserom indukovaná magnetizácia, pulzný laser

Keywords
Data storing, Fe-Rh, magnetostructural phase transition, laser induced magnetization, pulsed laser

VELIČ, A. *Optical study of laser-induced magnetic phase transitions*. Brno: Vysoké učení technické v Brně, Faculty of Mechanical Engineering, 2022. 42 s. Vedoucí M.Sc. Jon Ander Arregi Uribeetxebarria, Ph.D.

BRNO UNIVERSITY OF TECHNOLOGY
FACULTY OF MECHANICAL ENGINEERING

Assignment Bachelor's Thesis

Institut:	Institute of Physical Engineering
Student:	**Alexander Velič**
Degree programm:	Physical Engineering and Nanotechnology
Branch:	no specialisation
Supervisor:	**M.Sc. Jon Ander Arregi Uribeetxebarria, Ph.D.**
Academic year:	2021/22

As provided for by the Act No. 111/98 Coll. on higher education institutions and the BUT Study and Examination Regulations, the director of the Institute hereby assigns the following topic of Bachelor's Thesis:

Optical study of laser–induced magnetic phase transitions

Brief Description:

Metamagnetic materials display a phase transition from a low magnetization (e.g., antiferromagnetism) to a high magnetization state (e.g., ferromagnetism) upon an external trigger, such as a temperature change or an applied magnetic field. This bachelor thesis deals with the optical study of the antiferromagnetic–to–ferromagnetic phase transition induced by ultrashort laser pulses in metamagnetic nanoscale systems. In particular, metallic alloys with bistable antiferromagnetic and ferromagnetic phases at room temperature will be fabricated using thin film deposition. The laser–induced local writing of magnetization will be investigated for different samples and experimental settings.

Bachelor's Thesis goals:

1. Literature research of the state–of–the–art on the topic and related methodologies.
2. Preparation and basic characterization of metamagnetic samples (thin films or patterned structures) with a bistable antiferromagnetic and ferromagnetic state at room temperature.
3. Optical and magneto–optical imaging of the laser–written magnetic domains for different laser illumination conditions.

Recommended bibliography:

BERGMAN, B. et al. Identifying growth mechanisms for laser-induced magnetization in FeRh. Physical Review B. 2006. 73, 060407(R). ISSN 2469-9969. Dostupné z: doi:10.1103/PhysRevB.73.060407

ARREGI, J. A., CAHA, O., a UHLÍŘ, V. Evolution of strain across the magnetostructural phase transition in epitaxial FeRh films on different substrates. Physical Review B. 2020. 101, 174413. ISSN 2469-9969. Dostupné z: doi:10.1103/PhysRevB.101.174413

MEI, A. B., et al. Local Photothermal Control of Phase Transitions for On-Demand Room-Temperature Rewritable Magnetic Patterning. Advanced Materials. 2020. 32, 2001080. ISSN 1521-4095. Dostupné z: doi:10.1002/adma.202001080

Deadline for submission Bachelor's Thesis is given by the Schedule of the Academic year 2021/22

In Brno,

L. S.

prof. RNDr. Tomáš Šikola, CSc. Director of the Institute	doc. Ing. Jaroslav Katolický, Ph.D. FME dean

I hereby declare that I have written my bachelor's thesis with assignment of Optical study of laser-induced magnetic phase transition independently, under the guidance of my supervisor M.Sc. Jon Ander Arregi Uribeetxebarria, Ph.D., and using sources quoted in the list of literature at the end of the thesis.

Alexander Velič

I am immensely grateful to my supervisor M.Sc. Jon Ander Arregi Uribeetxebarria, Ph.D. first for inspiring me to work on this topic and to keep trying even when experiments would not go as planned, for his relentless support, ability to explain and spark interest in many topics along the way and of course for valuable advice given at noon or 3 AM and also for finalizing samples.

Many thanks also to my colleague Jakub Opršal for his friendly support in the laser lab and for being such a great lab partner.

I would also like to thank the whole CEITEC magnetism group for allowing me to utilize the equipment to its fullest potential and of course many thanks to magnetism group leader Ing. Vojtěch Uhlíř, Ph.D. Secondy I thank the whole CEITEC organization for letting me be part of their ranks. CzechNanoLab project LM2018110 funded by MEYS CR is gratefully acknowledged for the financial support of the measurements and sample fabrication at CEITEC Nano Research Infrastructure.

Goes without mention, but I am also incredibly grateful for my friends who have made this journey even more enjoyable.

Alexander Velič

Contents

Introduction

In past hundred years, technology has relentlessly gotten faster with each passing decade. Modern age is immensely swift and the demand for the ever-increasing speed of processes is higher than ever. As electronic industry is now successfully entering nanoworld, as predicted by Moores's law, modern computers commonly reach clocking speeds of few GHz. However, data storing capability lacks behind, requiring few nanoseconds. This discrepancy in speeds leads to a rise of ultrafast technology gap which is an issue for IT industry. Simply put, there is substantial need for speed. The field of ultrafast magnetization is thus fiercely investigating ways of achieving speeds thought to be impossible before. Research of past few decades offered a suitable solution, the field of ultrafast magnetism has made possible magnetization manipulation in the picosecond time scale and below.

Present study introduces a promising aproach of executing such ultrafast magnetization. Utilization of special materials capable of laser induced metamagnetic phase transition from antiferromagnetic to ferromagnetic state is suggested. Such suitable material is FeRh alloy, which is capable of laser induced magnetization and subsequent retention of induced ferromagnetic bistability. Further tuning of transition temperature is possible, thus granting FeRh samples the capability of retaining ferromagnetism at approximately room temperature. This thesis focuses on fabricating suitable FeRh thin films capable of sustaining magnetization at room temperature. This property is achieved by utilizing phase transition tuning techniques. Subsequent goal is to characterize and investigate phase transitions in specific samples and to gain deeper understanding of *how* and more importantly *when* they arise. To accommodate ability to switch polarization by using incident laser pulses, the laser irradiation experimental set-up was build, The magnetic states of FeRh thin films induced by laser irradiation are studied.

Chapter 1 provides a summary of past and current research in the ultrafast magnetization field. In chapter 2 a brief overview of basic principles of magnetism theory is provided, with focus on models fundamental for understanding of performed experiments. Chapter 3 is dedicated to explanation of crucial concept of magnetostructural phase transition. This concept is then expanded on in Chapter 4, where Iron-Rhodium material is introduced. Chapter 5 discusses basic principles of experimental methods utilized in the experiments. Main focus of Chapter 6 is to describe FeRh thin films preparation and their characterizations by using magnetometry and microscopy and subsequently to report the results and observations. Final experimental Chapter 7 offers the laser induced magnetization experiment and acquired results.

1. Laser induced magnetic phase transitions

On the verge of new millenia, E. Beaurepaire studied ultrafast spin dynamics in a Ni thin film using femtosecond optical pulses. It was proven that a femtosecond optical pulse can induce a nascent nonequilibrium electron gas which thermalizes to a Fermi distribution within 500 fs [1]. Thermalization happens due to electron-electron interaction. The hot electron gas transfers its energy to the lattice via electron-phonon interactions within first 1-10 ps. After the first pulse arrives, it was observed that magnetization of the sample abruptly dropped within first picosecond after the excitation, thus proving the demagnetizing effect of ultrashort optical pulses on ferromagnetic materials. During the study of ultrashort optical pulse affects on magnetic system, a three interaction reservoir phenomenological model was developed. It states that energy pumped into the system via ultrashort laser pulses excites electrons first (electrons are the fastest to react) with a subsequent energy transfer and relaxation between three interaction reservoirs: electrons (electronic population), spins (magnetic system) and phonons (lattice).

This work described a substantial breakthrough, ultrafast demagnetization of a ferromagnetic material (Ni) was proven to be possible. Figure 1.1 proves that magnetization drop took place within first picosecond. This experiment is considered to be the beginning of the research field of ultrafast magnetism.

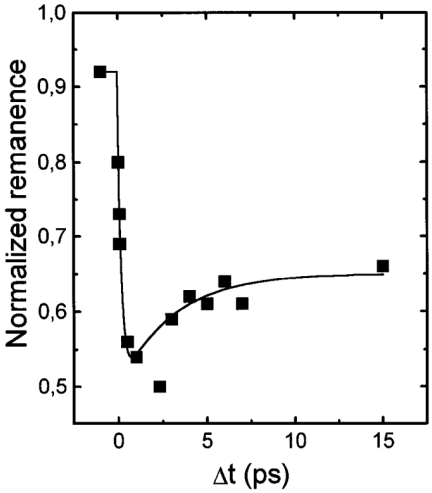

Figure 1.1: Adapted figure form [1] shows rapid magnetization decrease after initial laser pulse arrived.

As suggested in motivation at the beginning of this chapter, field of ultrafast magnetism has extensive application in memory storage systems. Magnetic based storage devices use logical bits, ones and zeros, to store data. Conventional approach for writing ones and zeros is to set magnetization vector of a given magnetic domain to be ”up” or ”down” . However an alternative use of domains exhibiting magnetization (ferromagnetic domains) as ones and antiferromagnetic domains as zero, might be adapted. Modern devices use magnetic field antiparallel to magnetization vector of a given domain, thus reversing the magnetization and writing down a single bit of information [2]. Much faster

reversal can be accomplished when magnetic field is being applied perpendicular to magnetization vector via precessional switching [3]. Notwithstanding the higher speed achieved, a recent study concluded that sub 2 ps deterministic precessional switching is not possible [4]. Following studies have since been looking into a suitable, much faster alternative. As already hinted before, ultrafast optical magnetization was found to have a advantageous characteristics, much needed for further development of ultrafast magnetic based storage systems.

Subsequently in 2007 C. D. Stanciu and coworkers found that the magnetization of ferrimagnetic material can be reversed or switched, using single ultrashort laser pulses of circularly polarized light in the absence of any external field [5]. Which was thought to be impossible before. The circularly polarized electro-magnetic waves acted on magnetic systems as short lasting magnetic fields. Left and right circularly polarized electromagnetic waves act as a magnetic fields with opposite signs [6]. Incident photons cause optical excitation and consequent ultrafast heating of the magnetic system just below Curie point. This leads the system to an unordered state which is highly susceptible to magnetic field simultaneously generated by the circularly polarized incident light pulse. Helicity of the polarized light is then the determining factor for the direction of this optomagnetic switching. This study demonstrated that a single 40 fs laser pulse was therefore able to cause permanent magnetization reversal. Such permanent magnetization reversal was also performed in material suitable for data storage. Such proof of ultrafast magnetization switching was another imperative step for development of technologies capable of writing magnetic bits at ultra-fast speeds

In 2010 Kirilyuk expanded on the explanation of laser pulse manipulation of magnetic systems [7]. The work proposed explanation of an underlying mechanism of photon interaction with aforementioned interaction reservoirs; charges, spins and lattice itself shown on fig.1.2, and angular momentum transfer between them. Three main classes of photon effects on magnetic systems were introduced; thermal effect, nonthermal effect and nonthermal optomagnetic effect.

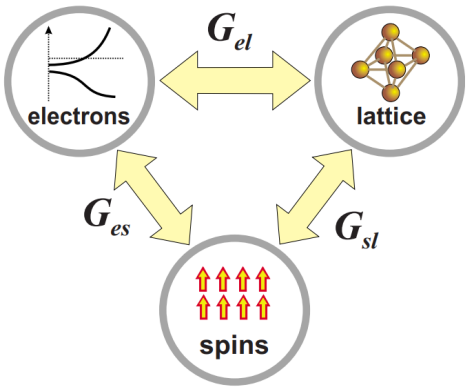

Figure 1.2: Triple reservoir concept showing different energy relaxations paths. Where G_{ij} represents coupling between individual reservoirs. Adapted from [7]

Moreover Kirilyuk studied timescales at which individual processes of energy relaxation take place once photon pumps energy into the magnetic system (see Figure 1.3).

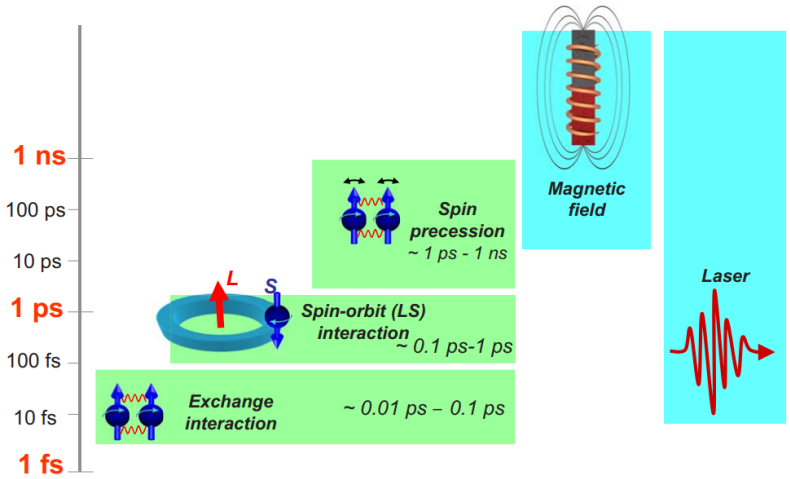

Figure 1.3: Diagram shows different time scales of individual interactions in magnetism, in comparison laser pulses and magnetic field. Adapted from [7].

Study shows that laser pulses are able to affect magnetization on much shorter time frames, than magnetic field. Suggesting that laser induced magnetization might be suitable for ultrafast storage of information.

2. Magnetism

In order to explore magnetic properties and investigate corresponding phenomena, a brief look into the fascinating world of magnetism is included below. Following theoretical chapters aim to develop basis of explanation for later introduced magnetic experiments.

2.1. Magnetic field and magnetization

Magnetic behavior of a material can be described using set of physical properties. First of which is *magnetic field* B, which is, according to Maxwells equations, divergenceless. Gausss law states,

$$\nabla \cdot \mathbf{B} = 0 \tag{2.1}$$

there can be no sources and no sinks of *magnetic field* B. Visualization of magnetic field can be done using closed loops representing force lines of B. Therefore no magnetic monopoles can exist. Using SI system we quantify magnetic field using units, which correspond to $kgs^{-2}A^{-1}$.

Magnetic field strength H offers different approach in describing magnetic fields. Local value of H-field is reflected by the magnetization of a solid and is therefore essential when describing magnetic fields in solids. Relation between magnetic field and its strength is trivial. When it comes to free space, it is given by a constant know as magnetic permeability μ_0 [8],

$$\mathbf{B} = \mu_0 \mathbf{H} \tag{2.2}$$

H-field is described using SI units as Am^{-1} . In materials the description of the magnetic field gets complicated. Using differential form of Ampers law, curl of B is now rewritten using total current density,

$$\nabla \times \mathbf{B} = \mu_0(\mathbf{j}_c + \mathbf{j}_m) \tag{2.3}$$

where j_c is conduction current and j_m represents Amperian magnetization current proportional to magnetized material. Amperian magnetization current is very useful tool in describing magnetized material, since it is responsible for generating materials magnetization. Although it cannot be measured, it can be described using measurable quantity M known as *magnetization vector field* as,

$$\mathbf{j}_m = \nabla \times \mathbf{M} \tag{2.4}$$

where magnetization is defined as net *magnetization moment* μ_i per unit of volume V,

$$\mathbf{M} = \frac{\sum_i \mu_i}{V} \tag{2.5}$$

Using SI units the description of M is the same as for H-field, Am^{-1}. Magnetization is essential for describing the impact of magnetic field on solids. However it also serves as

a indicator of magnetic state of a given solid, as will be closely explained in the chapter 2.5.

Dipole magnetic moments are an elementary quantity in solid-state magnetism. Magnetic moments are associated with electron spins and with electron orbital motion around the nucleus. Both spin and orbital moments add up in ways allowed by the laws of quantum mechanics. Most of the moments cancel out and only few atoms thus posses resultant magnetic moment. One can then define local magnetic moment density and describe the magnetic configuration system using local magnetization function $M(r)$.

Expression (2.6) can then be rewritten as following,

$$\mathbf{B} = \mu_0(\mathbf{M} + \mathbf{H}) \tag{2.6}$$

Further connections can be made between magnetization and H-field using a constant know as *magnetic susceptibility* χ ,

$$\mathbf{M} = \chi\mathbf{H} \tag{2.7}$$

Magnetic susceptibility describes the behavior of a material when an external magnetic field is present. Materials can then be separated into groups, depending on response to external magnetic field (depending on the susceptibility values)

Subsequently we can describe magnetic field in materials using previous expressions,

$$\mathbf{B} = \mu_0(1 + \chi)\mathbf{H} = \mu_0\mu_r\mathbf{H} \tag{2.8}$$

where *relative permeability* has been defined as,

$$\mu_r = (1 + \chi) \tag{2.9}$$

2.1.1. Magnetic domains

In materials which exhibit spontaneous magnetization (such as ferromagnets), magnetic configuration system can be understood as system of uniformly magnetized regions. Meaning in these regions magnetic moments are aligned parallel to each other along a single axis. These uniformly magnetized regions are known as magnetic domains [9], hinted in the top part of fig.2.2c. The presence of these magentic domains is a result of dipolar interactions, liable for magnetostatic energy contributions. The direction of magnetization of constituent domains and their shape are defined by minimizing the free energy of the system, as will be discussed in the following chapter.

2.2. Energy of magnetic systems

In nature, all things strive to achieve a state with minimum energy. The same can be said about magnetic domain structure. The orientation of magnetic domains will always form in such a way that the total free energy is reduced to either local or global minimum. Total free energy ε_{tot} of the single domain system may be written as a sum of partial energy terms,

$$\varepsilon_{tot} = \varepsilon_{EX} + \varepsilon_A + \varepsilon_D + \varepsilon_Z \tag{2.10}$$

where the first three terms are energy contributions due to *exchange* ε_{EX}, *magnetocrystalline anisotropy* ε_A, and *demagnetizing field* ε_D. These terms are always, to some extent, present when considering ferromagnets. Term ε_z is considered when an external field is applied and describes magnetic processes and hysteresis loop, it is know as the Zeeman energy term. By fully understanding history of the system and the energy terms of a domain structure in an external field, we are in theory able to determine the orientation of its magnetization.

Exchange energy

Consider two particles with a spin value of $s = 1/2$ are coupled with interaction described by a Hamiltonian [9],

$$\hat{H} = A\hat{S}^a\hat{S}^b \tag{2.11}$$

where $\hat{S}^a$ and $\hat{S}^b$ represent spin operator for the two particles, and A is a exchange stiffness. By combining the two particles together resulting joint entity has two possible values of quantum spin number $S = 1$ or 0 . Where state with $S = 0$ is a singlet resulting in an energy value of $-3A/4$. Whereas the state with the value $S = 1$ is a triplet and results in a higher energy value $A/4$. The system can be described using a wave function which must be anti-symmetric with respect to exchange of the two electrons. Wave function can be written as a combination of a spatial wave function and spin wave function, where spin wave function is a linear combination of all possible states. In order to satisfy exchange asymmetry of the total wave function, whatever the exchange symmetry of spatial wave function, the spin wave function has to have opposite exchange symmetry. Hence the spin wave function must be symmetric ($S = 1$) in a case of spatial wave function being anti-symmetric. Therefore only symmetrized or antisymmetrized states are allowed. Two possible wave functions ψ for singlet and triplet and energy E of their states are,

$$E_S = \int \psi_S^* \hat{H} \psi_S \, dr_1 \, dr_2 \tag{2.12}$$

$$E_T = \int \psi_T^* \hat{H} \psi_T \, dr_1 \, dr_2 \tag{2.13}$$

Hence the Hamiltonian can now be written in the form of an effective Hamiltonian $\hat{H}$,

$$\hat{H} = \frac{1}{4}(E_S + 3E_T) - (E_S + E_T)S_1 \cdot S_2 \tag{2.14}$$

It is a sum of a constant term and spin dependent term. It can be rewritten using exchange integral,

$$J = \frac{E_S - E_T}{2} = \int \psi_a^*(r_1)\psi_b^*(r_2)\hat{H}\psi_a(r_2)\psi_b(r_1) \, dr_1 \, dr_2 \tag{2.15}$$

As following,

$$\hat{H}^{spin} = -2J\mathbf{S}_1 \cdot \mathbf{S}_2 \tag{2.16}$$

when considering more than two spins, all can be easily applied using Heisenberg model,

$$\hat{H} = -\sum_{ij} J_{ij} \mathbf{S}_i \cdot \mathbf{S}_j \tag{2.17}$$

where J_{ij} is also known as exchange constant. Positive exchange constant indicates that parallel alignment of neighbor magnetic spins is favorable, distinctive for ferromagnetic systems. In contrary, negative exchange constant points to a antiparallel alignment, preferred by antiferromagnetic systems.

This is particularly useful when considering multiple electron model, where electrons belong to different atoms, such as in lattice atoms of a ferromagnetic material. When angle deviation of two electron spins in question θ_{ij} is small enough, the energy of the system can be written as,

$$E = -JS^2 \sum_{ij} \cos\theta_{ij} \tag{2.18}$$

In continuum limit we ignore the discrete nature of the lattice and rewrite exchange energy term as following,

$$\varepsilon_{EX} = \int A \left(\frac{\nabla \mathbf{M}}{M_s} \right)^2 d^3r \tag{2.19}$$

where M/M_S is an unit vector in the direction of local magnetization. Then the divergence of this vector could be understood as misalignment of neighboring magnetic moments. The constant A is already mentioned exchange stiffness.

When system finds itself in a global energy minimum, the energy minimum of exchange energy term favors a state with smoothest possible variation of vector M/M_S in all directions. Depending on the sign of exchange stiffness A, parallel moment orientation (ferromagnetism) or antiparallel moment orientation (antiferromagnetism) is favorable. Exchange interaction can generally be considered as the reason for magnetic moments alignment, and thus formation of magnetic domains.

Ferromagnets and antiferromagnets were not fully understood for a quite some time. As demonstrated in this chapter, explanation for ferromagnetic and antiferromagnetic order requires quantum mechanics and the concept of exchange interaction. Proposal of exchange interaction by Heisenberg was derived from fundamental concepts of Coulomb interaction and Pauli exclusion principle. Quantum mechanics was also needed to prove the condition of the symmetry properties of multiparticle wave functions.

Magnetocrystalline anisotropy

In certain crystallographically ordered materials, there are lattice orientations which are energetically more favorable in terms of magnetic moment alignment. These favorable lattice orientations are known as easy axis. Depending on the crystalline structure there can be multiple easy axis. The magnetocrystalline anisotropy energy term dictates that domain magnetization direction aligns along one of the easy axis, in order to achieve energy minimum. The combination of both magnetocrystalline anisotropy term and exchange term lead to a domain structure, where the magnetization follows the easy axis direction

and individual domains are divided by narrow domain walls, where magnetization direction slowly switches from one easy axis to another. For a material with a single easy axis (uniaxial anisotropy) the energy demand of a certain orientation can be expressed using formula

$$\varepsilon_A = \iiint_V K_u \sin^2\theta \, d^3r \tag{2.20}$$

where θ is the angle between easy axis and the vector of magnetization, K_u is known as anisotropy constant [10].

Demagnetizing field energy term

Also known as dipolar energy term is caused by magnetic dipole-dipole interaction of the magnetic moments within the magnetic system. This interaction is based on interaction of a given magnetic moment with the magnetic field generated by adjacent magnetic moments. This mutual affect of adjacent moments on each other tends to demagnetize the body by splitting it into regions with different magnetization orientation. Thus effectively forming aforementioned magnetic domain structure. Demagnetizing field energy contribution can be written as a following integral over the volume of the magnetic material,

$$\varepsilon_D = -\frac{1}{2}\int \mu_0 \mathbf{H}_D \cdot \mathbf{M} \, d^3r \tag{2.21}$$

Demagnetizing field H_D is induced by virtual magnetic charges, which are considered when M is pointing out or in of a surface boundary. Hence, the demagnetizing energy increases when M points in or out of the surface boundary.

Zeeman energy term

When external magnetic field H_{ext} is applied, it induces a torque Γ upon magnetization M,

$$\Gamma = \mu_0 \mathbf{M} \times \mathbf{H}_{ext} \tag{2.22}$$

External magnetic field is thus forcing magnetization to align itself with the direction of applied external field. Misalignment of magnetization and external field increases energy of the system. The Zeeman energy term can be expressed using following volume integral,

$$\varepsilon_Z = -\mu_0 \iiint_V \mathbf{M} \cdot \mathbf{H}_{ext} \, dV \tag{2.23}$$

where ε_Z is minimal when M is aligned parallel to the direction of external field H_{ext}. In conclusion, due to Zeeman energy term, magnetization reversal can be performed using strong enough field.

2.3. Energy landscape of magnetic systems

Previously described energy states are often metastable, such states have higher energy than the global energy minimum for the given configuration of external or internal factors. Meaning, system can easily get trapped on a plate-like energy landscape or local minimum, representing seemingly random orientation of the magnetization domains. The energy landscape can be manipulated using various external physical quantities, such as temperature or magnetic field. Suppose an energy landscape of a the magnetic system. By applying external magnetic field, the energy landscape of the previously stable system will alter. Landscape represented by figure 3.1 shows a magnetic system (blue ball) being stuck on a metastable energy state (magnetization vector of the studied domain is random) when there is no external field present. However when external magnetic field is applied (pointing down) energy landscape of the system begins to shift. Suddenly the state in which domain currently exist becomes even more metastable, and even more energy demanding for the system. In the contrast, state with magnetization vector parallel to the vector of magnetic field becomes more favorable for the system. When the applied magnetic field is further increased, the initial state becomes so energy demanding that the state is no longer able to sustain it and is thus forced to change it. Magnetization orientation changes, and state thus drops into a global energy minimum. The global energy minimum state being a state where magnetization of the domain points parallel with the applied field. This illustration was concerned only with orientation of magnetization within one domain, but shape, growth, interaction with other domains and essentially the whole magnetic system can be described in similar fashion using the understanding of main energy terms of the system as described in the chapter 2.2

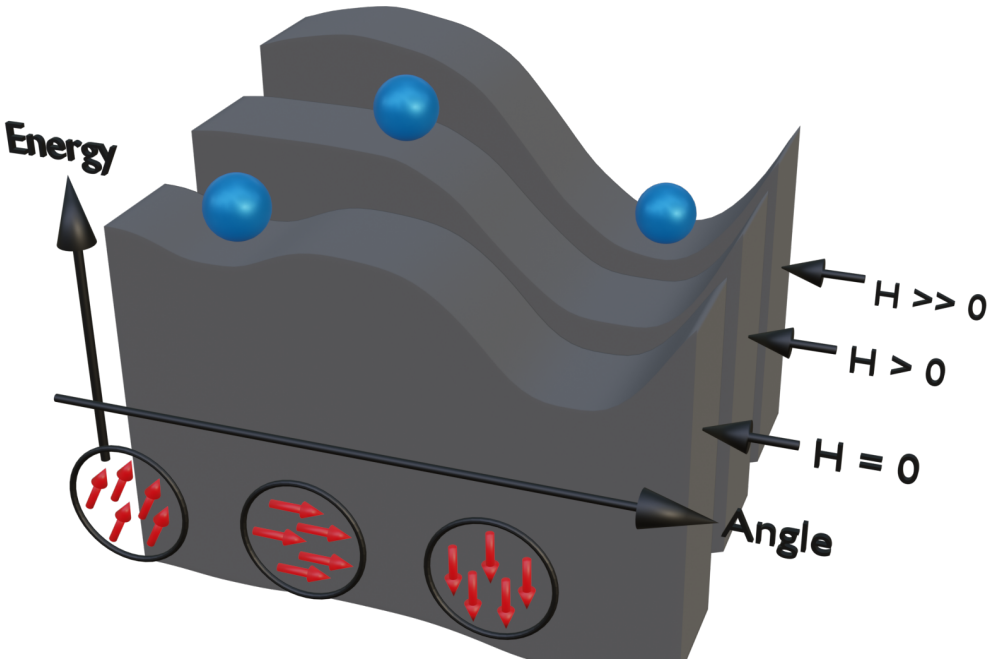

Figure 2.1: Release from metastable energy state.

2.4. Effects of laser pulse on magnetic system

It has been proven that deterministic magnetization reversal is unable to occur if the magnetic field pulse is sub 2 ps [4]. Possibly a laser pulse might be a useful alternative for ultrafast magnetization. Ever since Beaurepaire has demonstrated subpicosecond demagnetization using a laser pulse [1], ultrafast magnetization dynamics field has been researching magnetic systems as energy and spin/orbital momentum are exchanged between thermodynamic reservoirs of the system. Femtosecond laser pulse causes a highly nonequilibrium state in a magnetic medium [5, 1, 14]. The magnetic phenomena are thus no longer describable by equilibrium thermodynamics theory. At shorter time scales, magnetic anisotropy and spin exchange interaction should be considered as time dependent, which complicates analytical description of this issue.

Ultrafast optical control of magnetization is a result of mainly these three phenomena: spin-lattice, spin-orbit and electron-lattice interactions [7]. Drivers of magnetization when using pump laser pulses can be categorized using one of the following cases;

Thermal effects

By the means of absorbed photons the energy is pumped into the system. Magnetization is then function of a spin temperature $M = M(T_s)$. Light pulses pump energy into the electron-phonon system. Resulting magnetization has a time frame, which depends on internal equilibrium processes (electron-electron, electron-phonon and electron-spin interactions). Time frame can get as short as 50 ps. In real materials, thermal effects are always present.

Photomagnetic (nonthermal) effects

Incident pulses of photons are absorbed by electronic states which have direct influence on magnetic parameters, such as, magnetocrystalline anisotropy. These parameters cause a change of magnetic moments direction that obey precession behavior.

Optomagnetic (nonthermal) effects

These effects do not require absorption of photons and are in contrast with previous situation caused by a optically coherent stimulated Raman scattering. Driving force of magnetization change is due to spin-orbit coupling. Subsequent change induced by this mechanism can be considered to be instantaneous.

In order to fully understand physical properties of a material, one must understand the behavior of systems' degrees of freedom at microscopic scale. Equlibrium state may be disturbed and degrees of freedom altered using external parameters, such as magnetic field or temperature. External parameters may drive phase transitions and thus alter materials physical properties. Recent studies have researched ultrafast photo-induced phase transitions constituted using a ultra-short laser pulses [5, 1, 14, 11]. Phase transition can be achieved by targeting a responsive degree of freedom, such as spin. Delocalized optical electron excitation reshapes relative electronic structure of bonding and antibonding bands. Portion of excited electrons n_e is now a control parameter which gradually

changes potential energy surface of the local system. This change of potential energy is due to ultrafast thermalization of electrons and subsequent alteration of Fermi-Dirac distribution.

2.5. Magnetic ordering

Magnetic materials are differentiable according to their magnetic structure in the state of minimum energy and also according to their behavior once exposed to an external magnetic field. This response is to external magnetic field is described by equation 2.7. Based on the value of magnetic susceptibility, most materials fall into one of these categories or their subcategories:

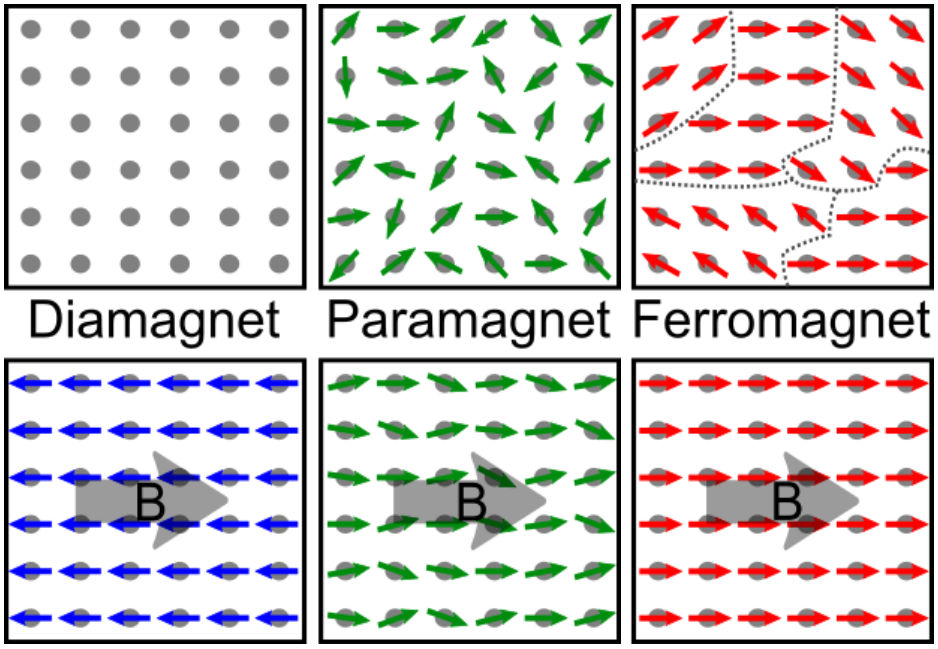

(a) (b) (c)

Figure 2.2: Representation of 2.2a diamagnetic, 2.2b paramagnetic and 2.2c ferromagnetic materials. Top parts of the figure illustrate magnetic moment structure of magnetic materials with absence of external magnetic field. Bottom part shows ordered magnetic moment structure when external magnetic field B is applied.

Diamagnetic materials

When external magnetic field is applied to a material, a change will be induced upon its atom orbitals motion. This orbital motion deviation due to an applied external field is known as diamagnetic effect. Diamagnetic effect is exhibited by all atoms regardless of their electron configuration. However, it's such a weak phenomenon compared to other interactions, that only materials, which have no magnetic moment caused by their filled electron orbital shells 2.2a, are classified as diamagnets. Once external field H_{ext} is applied to a diamagnet, its magnetic dipole moments orient themselves antiparallelly to the direction of H_{ext} as seen on the bottom part of the figure 2.2a. Diamagnets exhibit internal magnetic field opposite to the external field by which the internal moment was

induced. Magnetization vector thus points in opposite direction of H_{ext}, and is inversely proportional to applied magnetic field. This means that diamagnetic susceptibility must be negative. Diamagnets lose their magnetization once the external magnetic field is reduced to zero.

Paramagnetic materials

On contrary to diamagnetism, paramagnetism is exhibited only by materials of which atoms have unpaired electrons. Therefore they have a magnetic dipole moment on their own, even if no field is applied. These magnetic moments are weakly coupled to each other and so thermal energy causes magnetic moments to be randomly oriented throughout the system 2.2b. The system, therefore, does not exhibit any spontaneous net magnetization. However, when external magnetic field H_{ext} is applied, magnetic moments start to partially align in the direction of H_{ext} as seen on the bottom part of the 2.2b. Some net magnetization is then being observed. Magnetization M is thus directly proportional to external magnetic field H_{ext}, meaning that the susceptibility is slightly greater than zero [8]. For low enough magnetic fields the susceptibility χ is temperature T dependent with a relation described by Curie law:

$$\chi(T) \sim \frac{1}{T} \tag{2.24}$$

Ferromagnetic materials

The characteristic and also most important feature of ferromagnets is spontaneous net magnetization, which exist even if there is no external magnetic field present. Reasoning behind this spontaneous magnetization existence was briefly mentioned in the previous chapter and is explained by the positive exchange interaction (chapter 2.2). Positive exchange interaction ($J > 0$) causes parallel alignment of magnetic adjacent moments along a single direction, known as easy axis in a small region. Magnetic dipole-dipole interaction are thus responsible for formation of magnetic domains, shown on the top part of figure 2.2c. Domain structure of ferromagnets is temperature dependent because thermal fluctuation disorients individual magnetic moments. Response of ferromagentic materials to applied external magnetic field can be described using a hysteresis curve. Field driven hysteresis curve depicts dependence of magnetization M on external magnetic field H_{ext} (Figure 2.3). When ferromagnetic material is in a initially non-magnetized state with no previous magnetic history (material was not subjected to an external field), magnetic domains may be oriented in such a way that the material exhibits no net magnetization. Partial magnetization of each of the domains is canceled out by a magnetization of oppositely oriented domain. Once the external magnetic field H_{ext} increases, all misaligned magnetic moments (within magnetic domains with misaligned magnetization) start to align parallel to applied magnetic field. Domains with magnetic moments initially oriented parallel with the magnetic field start to grow and consume adjacent domains. The growth continues with increasing field until all present domains are oriented parallel to the external field, this is illustrated on the bottom part of the figure 2.2c. Since all domain magnetization points in the same direction, net magnetization of the system is a sum of

partial domain magnetizations. Net magnetization thus reached so called saturation magnetization value M_s. As the external field is reduced from saturation, some constituent domain magnetization vectors rotate away from the external field direction. Net magnetization thus drops to a remnant magnetization value M_r when external field drops to zero. Subsequently, in order to bring net magnetization of the system to zero, external field with value $-H_c$ needs to be applied. This characteristic values is known as coercive field. When the field is further increased in the negative values, domains start to orient in the direction of the applied negative magnetic field. Material then reaches negative net magnetic saturation. Upon applying opposite magnetic field once more, complementary magnetization reversal takes place. The hysteresis loop closes once net magnetization reaches the values of M_s.

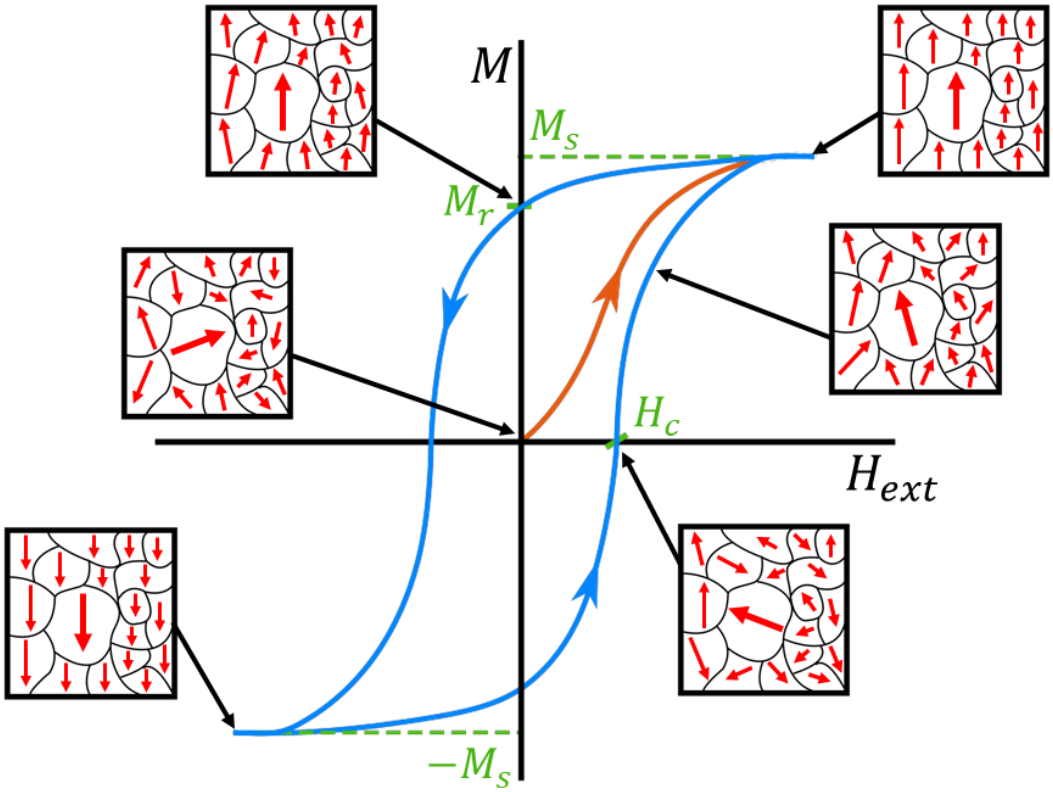

Figure 2.3: Magnetization reversal

Since thermal fluctuation randomize magnetic moments within the magnetic structure, magnetization of ferromagnets is immensely temperature dependent. If a ferrromagnetic system is heated up beyond a critical temperature T_C, known as Curie temperature, the ferromagnetic system undergoes a second-order phase transition and collapses into a paramagnetic state [8].

Antiferromagnetic materials

Exchange interaction in antiferromagnets tends to align adjacent magnetic moments antiparallel to each other. Antiferromagnetic system can be illustrated as two interpenetrating, identical sub-lattices of magnetic ions with antiparallel magnetic moments. When there is no external magnetic field applied, these antiparallel moments cancel each other out, therefore the system exhibits no net magnetization. The behavior of antiferromagnets is well described by their susceptibility temperature dependence. With increasing temperature, thermal fluctuations disorder the antiparallel system of magnetic moments, thus slowly promoting the increase in net magnetization. The susceptibility then increases with rising temperature, until temperature reaches critical values T_N, Neel temperature. At the value T_N, the antiferromagnetic state collapses and the material undergoes phase transition from antiferromagnetic to paramagnetic state. This transition is called Néel phase transition and may be achieved by a high enough temperature.

Certain materials that are AF at low temperatures can undergo a first-order phase transition to FM state (such as FeRh) upon increasing the temperature or applying a large enough magnetic field. These materials which undergo this first-order phase transition, for example Iron-Rhodium, their entropy, resistance, lattice volume, and most importantly magnetization also change.

3. Magnetic phase transitions

In previous chapter, magnetic system states and energy of these states were discussed. Brief description of different magnetic orders was given. The concept of changing these magnetic states was introduced by describing the behavior of domains which reflect these magnetic order states. For complete understanding of the physics behind experimental principles, it is crucial to further describe the change in magnetic states of the system and drivers behind mentioned change, also known as a phase transition.

3.1. Phase transitions

Phase is characterized by a thermodynamic function, which is the function of macroscopic parameters. These parameters can be various physical quantities. The order parameter is an especially important quantity, it measures the extent to which macroscopic parameters are ordered, or in a comparable state [12]. When discussing magnetic materials, magnetization is a characteristic order parameter. Magnetization is a value describing the response of a material to magnetic fields. When microscopic physical attributes changes, alignment of electronic spins and macroscopic parameter changes. Consequently magnetization of the system arises. This is the phase transition.

Physics behind the drivers of phase transition can be described as a competition between the internal energy E and the entropy S of the system, together they represent *free energy* F of the system ,

$$F = E - TS \tag{3.1}$$

Where F is free energy and T is temperature. A competition between S and E represents the constant internal fight for dominance, internal energy favors order but on the other hand, entropy represents disorder. Depending on macroscopic parameters, one or the other dominates the system.

Generally speaking, there are two types of phase transitions, first-order and second-order phase transitions. The order depends on the derivative of the free energy F of the system. When the first derivative of the free energy returns discontinuity, the phase transition is known as first-order phase transition. However when the second derivative returns a discontinuity, the phase transition is known as continuous or second-order phase transition.

When discussing magnetic materials, we are mostly concerned about the change of magnetization of a system. Suppose that we have a completely negatively magnetizes sample (negative saturation value of magnetization $-M_s$ as explained in chapter 2.5) in a negatively pointing external magnetic field H_{ext} at a temperature under critical value T_C. The magnetization goes from negative to positive when opposite (positive direction) external field is applied. The transition happens quite rapidly, thus first derivative of free energy is discontinuous and therefore the transition is a first-order phase transition.

For a different experiment we now suppose that the temperature is above critical T_c and the magnetization is thus close to zero. When cooling down from temperature

$T > T_c$ magnetization changes from zero to a positive value continuously, thus exhibiting second-order phase transition.

3.2. Magnetization reversal

As explained in the previous chapter, a ferromagnetic specimen may have multiple local minima of E_{total} [8] in which seemingly random orientation of domains (magnetization of domains) may exist as as explained in chapter 2.3. We now presume that the system (blue ball) is in a stable energy minimum (magnetization points down) when no external field is present in Figure 3.1. All domains of the system are thus aligned and system posses net magnetization $-M_s$. In order to achieve magnetization reversal as hinted in the 2.5 magnetization value needs to be switched to $+M_s$. As soon as external magnetic field (pointing down) is applied, energy topography of the system starts to get altered. Initial state starts to be undesired for the system, since the energy value of that state increased. While the original system (magnetization pointing down) became more energy costly, state representing magnetization pointing down (magnetization parallel to the external field) became much more favorable. When the external magnetic field reaches switching field value H_S (highest slope point of field driven hysteresis), magnetization reversal process begins. The initial state becomes unsustainable for the system and is forced to change. Magnetization aligns itself with the external magnetic as the state drops into the global energy minimum. Further increase of magnetic field forces every domain into a state with minimum energy. Thus slowly concluding the magnetization reversal process as net magnetization reaches positive saturation value $+M_s$. The whole process can be viewed as an attempt of the system to preserve as low energy as possible, similarly to most processes in the nature. In following chapter we will discuss similar transition, known as metamgnetic phase transition, where similar energy topography concept can be employed. With a crucial difference being, that the energy landscape alternation will be possible using heat or ultra-short light pulses.

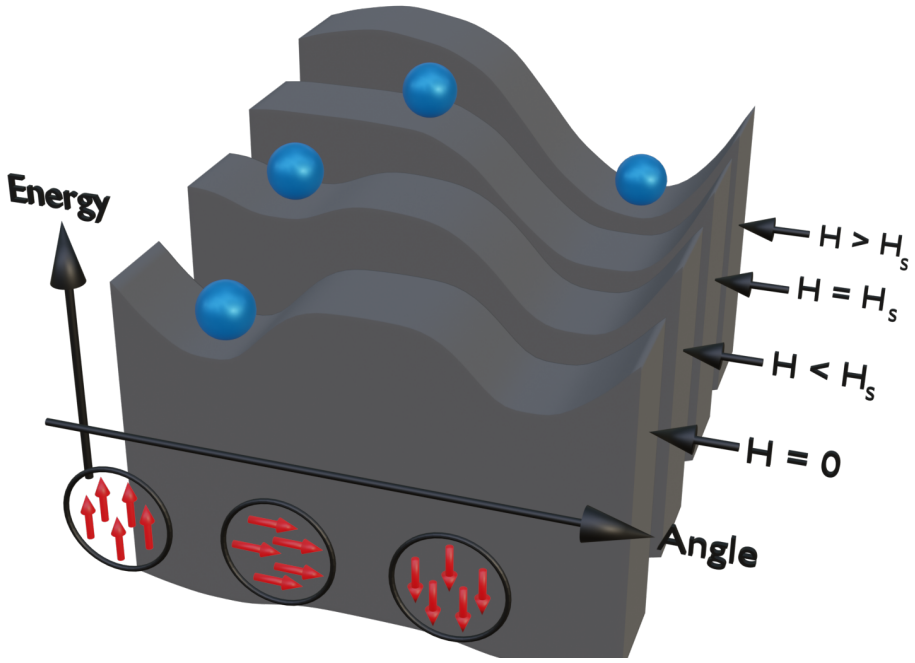

Figure 3.1: Energy landscape image describing how energy of a domain orientation state changes when magnetic field is applied. State of the system (symbolized by the blue ball) is forced into metastable states with higher energy when magnetic field is applied. System naturally prefers to be in a state with minimum energy. When sufficient field is applied (H_S), the system minimizes its energy by adapting the orientation (and shape) of the magnetic domain in response to the magnetic field.

4. Iron-Rhodium

Now with the understanding of magnetic phase transitions, special material which is the main focus of most performed experiments can be introduced. Although FeRh behaves slightly differently than phenomena described previously, the principle remains the same. Special properties of Iron-rhodium were discovered by M. Fallot in 1939 [13]. Iron-Rhodium exhibits fascinating metamagnetic property, FeRh is able to undergo a transition between *antiferromagnetic* (AF) and *ferromagnetic* (FM) states. Meaning, it undergoes transition from a state in which all constituent atomic magnetic moments cancel each other out, to a state where magnetic moments point in the same direction and net magnetization is thus at its maximum. This first-order AF-FM phase transition can be optically or thermally driven and is trivial for experiments performed. Magnetic phase transition can be done in reversed order, cooling down from FM state to AF state, therefore following a sample specific thermal hysteresis. Another very essential capability of Iron-Rhodium, is its tunability of transition temperature at which the aforementioned AF-FM transition takes place [14]. Meaning, that we are able to quite precisely set a temperature threshold at which we want the AF-FM phase transition to take place.

4.1. Magnetostructural phase transition of FeRh

As mentioned above, Iron-Rhodium is capable of first-order metamagnetic phase transition. Iron-Rhodium is an alloy and as such its phases can be well described by a phase diagram 4.1. $Fe_{1-x}Rh_x$ for $0.48 < x < 0.54$ at room temperature (300 K) sample is in a antiferromagnetic α'' phase. When heating up the system through transition temperature T_t, Iron-Rhodium undergoes a thermodynamic first-order antiferromagnetic to ferromagnetic phase transition (AF-FM). Transitioning through a phase where both AF and FM domains are present ($\alpha'' + \alpha'$) into a fully ferromagnetic α' phase [15]. While magnetic properties change drastically, structural change is also present and therefore the first-order AF-FM phase transition is denoted as a magnetostructural phase transition, which is also accompanied by a change in resistivity. More importantly reflectivity decreases by about 3 %, when AF-FM transition takes place [16]. Magnetostructural phase transition can, in addition to temperature, be induced using external magnetic field, strain or optical ultrashort pulses. During the magnetostructural transition first order derivative of Gibbs free energy, $G(T, S) = U + PV - TS$ (U => internal energy, S => entropy, V => volume and P => pressure) shows a discontinuity, underlining a strong coupling between orbitals and lattice and thus confirming magnetostructural nature of AF-FM transition [14]. If the system would have been heated even more, it would have undergone second-order phase transition at Curie temperature and thus become paramagnetic.

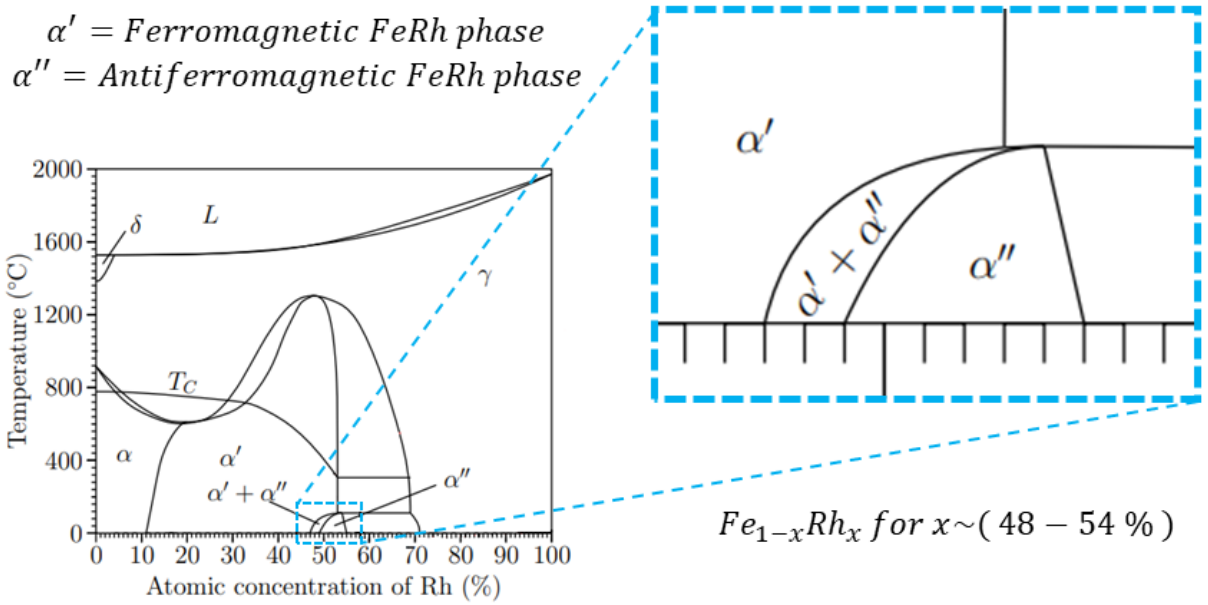

Figure 4.1: Phase diagram of FeRh adapted from [15]: α' - B2-ordered body centered cubic (BCC) FM phase, α'' - B2-ordered body centered cubic (BCC) AF phase, α - low temperature BCC phase, T_C indicated Curie temperature, γ - face centered cubic (FCC) paramagnetic phase, δ- high temperature body centered cubic (BCC) phase, L - liquid phase

Both ferromagnetic and antiferromagnetic phase posses the same crystallographic structure of B2-ordered $CsCl$-like body centered cubic (BCC) structure 4.2. Rh is central atom of BCC structure surrounded by Fe atoms. When in AF phase, Fe atoms exhibit antiparallel neighboring magnetic moments ($m = 3.3\mu_B$ per atom). In this AF state (left part of the figure), Rh atom posses no magnetic moment [17]. Once AF-FM phase transition takes place and FeRh is in a FM phase (right part of the figure), the magnetic moments of Fe atoms align parallel to each to each other (now exhibiting $m = 3.2\mu_B$ per atom). Consequently, magnetic moment is induced upon central Rh atom (possessing moment $m = 0.9\mu_B$)[18, 19] as seen in figure 4.2.

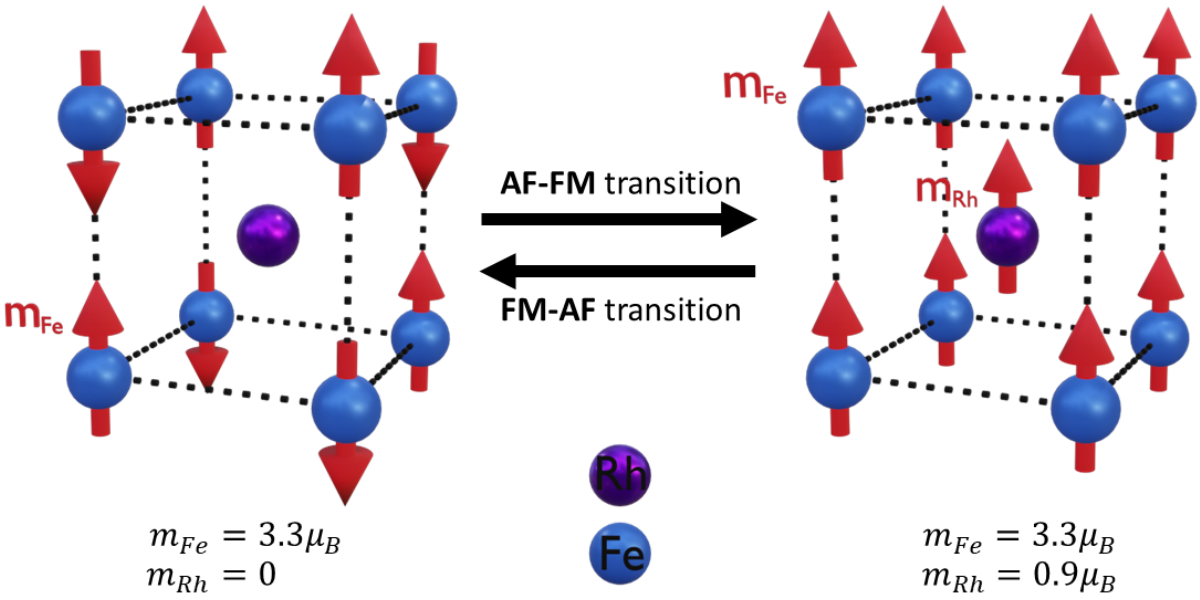

Figure 4.2: **Left** side of the figure shows magnetic moment structure of FeRh in **AF** state. **Right** side of the figure shows magnetic moment structure of FeRh in **FM** state.

4.2. Tuning of magnetostructural phase transition temperature

As discussed previously, the great virtue of Iron-Rhodium lies in the high tunability of temperatures at which already mentioned AF-FM and FM-AF phase transitions take place. This feat can be achieved mainly in three different ways. The most obvious one, since FeRh is an alloy, would be altering the composition within the mentioned range ($Fe_{1-x}Rh_x$ for $0.48 < x < 0.54$). This can be often complicated when trying to prepare thin films. Another easier method would be using lattice strain induced by a fitting substrate to shift the temperatures to our liking. It has also been shown that the phase transition temperatures are strongly affected by doping FeRh with a third element such as Pd, Pt or Al [20, 21, 15].

4.2.1. Tuning of transition temperature via element substitution

Substituting atoms of Rh in a bulk FeRH film results in a magnetostructural phase transition temperature alteration. Tuning transition temperature using this method was observed in 1966 by J.S. Kouvel [20] who utilized Pd, Pt and Ir doping. The focus of this work was on the magnetization change, variation of the entropy change during the transition and more importantly transition temperature shift. Results show that doping with Pt, Ir increases the transition temperature and in contrary doping with Pd decreases the

transition temperature. Moreover in 2013 R. Barua [21] carried out an extensive study of predicting the the temperature shifts when doping FeRh. Link between transition temperature change and average weighted valence bad electrons concentration was described.

4.2.2. Tuning of transition temperature via latteral in-plane strain

As already mentioned, during magnetostructural phase transition volume increase takes place. Although crystallographis structure stays the same a lattice parameter differs (volume expands by about 1%) [22]. Meaning that the AF phase lattice parameter is slightly smaller than that of FM phase. When concerned with FeRh thin films, the lattice parameter is largely affected by the crystalline structure of the substrate. The misfit of substrate and FeRh lattice cause lateral strain.

Strain effect when using $MgO(001)$ and $Al_20_3(0001)$ (sapphire) as a substrate was studied in 2005 by S.Maat [17] . Results of this work indicate that MgO substrate forces a minor expansion of out-of-plane lattice constant and a compression of in-plane lattice parameter in the FeRh thin layer (known as tetragonal distortion). In contrast, when using saphire as a substrate, in-plane lattice parameter is expanded and out-of-plane lattice parameter is compressed. Compression of out-of-plane stabilizes the FM phase.

The work showed that when FeRh thin-film is deposited onto a saphire substrate, the transition temperature is lower in comparison to using MgO as a substrate.

4.2.3. Tuning of transition temperature via FeRh composition alteration

Aforementioned magnetostructural phase transition in a $Fe_{1-x}Rh_x$ systems takes place in a limited composition range $0.48 \leqslant x < 0.54$ [15]. As phase diagram suggest, by altering the composition (the value of x) temperature point at which AF-FM and also FM-AF phase transitions takes place can also be altered. When sample in a fully antiferromagentic phase α'' is being heated up, eventually it will reach a threshold beyond which bot α'' and α' coexist (growth of ferromagnetic domains), this signalizes the start of the AF-FM phase transition. It is apparent that by tuning the value x, the point at which AF-FM transition takes places will correspond to a higher or lower temperatures.

4.3. Bistability of FeRh

When we take a closer look at temperature hysteresis of a specific $Fe_{1-x}Rh_x$ alloy, there is a temperature point at which both AF and FM states can coexist. Suppose that only a specific region of the system is heated above AF-FM transition temperature and is now in FM state. When the whole system, which is in a AF state except for the one FM region, is cooled down to a temperature which is just above the critical FM-AF transition temperature, the system will remain in this AF and FM coexisting state. The previously mentioned region stays FM. Meaning, at specific temperature the system can sustain both AF and FM state. This is known as bistability of AF and FM states. Utilization of already mentioned practices in chapter 4.2, we are able to tune not only temperature at which AF-FM and FM-AF transitions take place but consequently also temperature at which bistability of AF and FM states exists. It is favorable for our experiments to strive to

achieve bistability at room temperature ($T = 300\,\mathrm{K}$). Once such sample with bistability at around room temperature is produced, our experiments can be carried out without any additional temperature controlling apparatus. Making the experiments considerably simpler to perform and achieving greater result consistency.

5. Experimental methods

The experimental methods utilized for thin film sample fabrication and later characterization are presented in this chapter.

5.1. Magnetron sputtering

Magnetron sputtering is a physical vapor deposition method (PVD) [23]. Sputtered particles originate from a magnetron gun, as shown on Figure 5.1. The whole process starts with deposition chamber where sample growth occurs, such that adequate high-vacuum environment is obtained prior to deposition. Once the chamber is vented, Ar gas is introduced in the chamber. Neutral argon gas is then ionized using direct current (DC) voltage forming plasma of Ar^+ ions. Present electric field between target and substrate accelerates, now positively charged, Ar atoms towards the magnetron target where they impact on target surface of material intended to be deposited. Quite a few phenomena may occur when Ar^+ energetically collides with the target material, eroding the target and ejecting target atoms out of the target. However, most important is the emission of sputtered target material atoms and secondary electron emission. Target atoms are then ejected into the chamber and also towards the substrate itself. Upon contact with any surface they begin to form layers. Uniform deposition onto the substrate is ensured by a steady substrate plate rotation. The deposition rate depends heavily upon aspects of the environment in the chamber. Namely Argon pressure, DC voltage, erosion state of the target and the stability of the plasma state. For precise thin-film thickness deposition it is necessary to measure deposition rate for individual targets used. Deposition rate can be measured using quartz crystal microbalance. For acquiring more precise deposition rate value of certain targets one can use x-ray reflectivity measurements of calibration thin films deposited on a substrate. Using known time of deposition and measured thickness it is straight forward to calculate precise value of deposition rate. In addition magnetron sputtering system at CEITEC BUT (BESTEC magnetron sputtering) allows heating the sample during or after deposition up to 1250 K in order to improve the quality of epitaxially deposited films. After deposition is completed, BESTEC magnetron also allows for sample annealing process to improve the crystalline character of the deposited film.

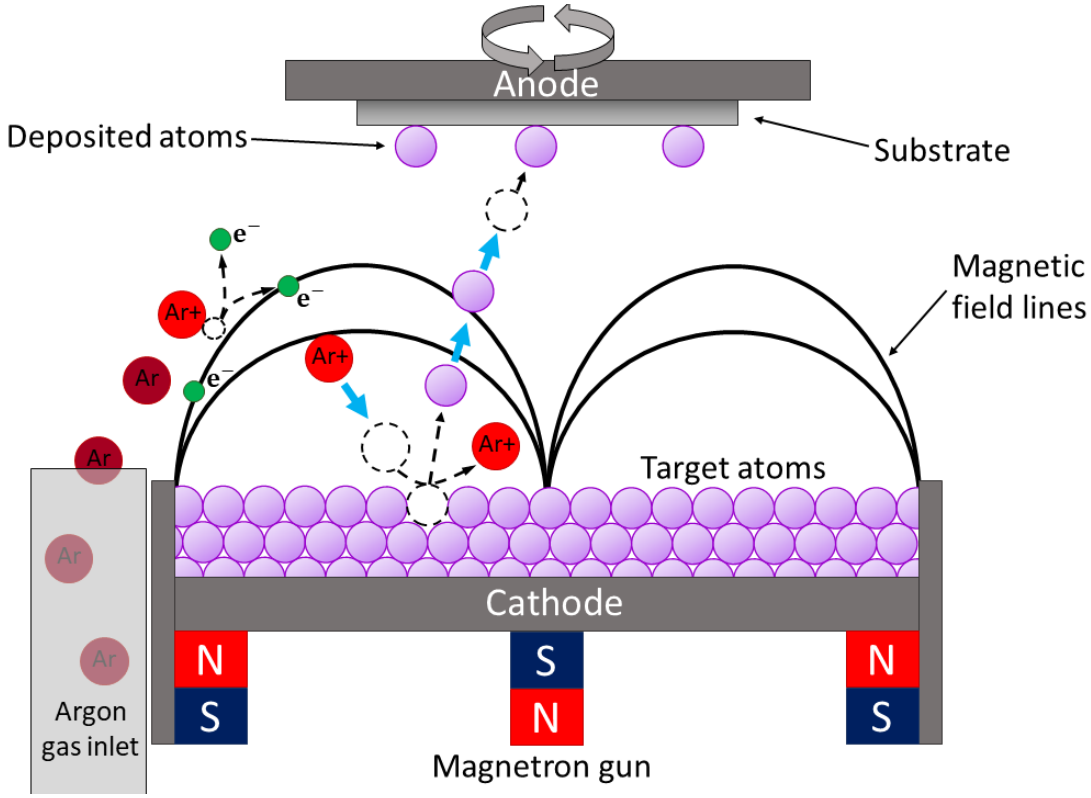

Figure 5.1: Schematic of the magnetron sputtering deposition process. Ar atoms are ionized and accelerated in high voltage towards a target of the material to be deposited. Ar+ ions erode and eject target atoms, which travel in all directions and are deposited on top of a substrate.

5.2. Vibrating sample magnetometry

In previous chapters a characteristic values of coercive field, remnant magnetization and saturation magnetization were introduced. These values combined with the characteristic hysteresis curve can be understood as a fingerprint of the magnetic material, which is specific for a given sample and are very important when characterizing samples used in later experiments. However, even more important characteristics values would be transition temperatures at which AF-FM and FM-AF phase transitions of FeRh take place. These characteristic values can be precisely measured using Vibrating sample magnetometry (VSM) depicted on figure 5.2.

VSM is a method used for quantifying the magnetic moment of the full volume of the tested sample. The VSM system at CEITEC BUT (Versalab by Quantum Design, Inc.) is capable of setting the sample temperature in the range 50-400 K and applying magnetic fields up to 3 T. Both parameters are essential for the sample characterization described in the later chapter. By turning on magnetic field inside testing chamber, magnetization parallel to magnetic field is induced within ferromagnetic regions of the sample. Vibrating motors of VSM force, now magnetized, sample into oscillating motion, generating time-variable stray magnetic field. Detection coils as detection system of the VSM are wound along the axis of the oscillating motion (as seen in Figure 5.2). Detection system picks-up electromotive force induced by the alternating magnetic field, which is

directly proportional to the net magnetic moment of the sample. Combining constant field and variable temperature inside the testing chamber, the temperature dependence of magnetization can also be recorded.

In the case of VSM measurements in magnetic thin films, one has to take into account the contribution of the substrate. Commonly used substrates are often diamagnetic (e.g., Si, MgO), where the application of magnetic fields produces oppositely oriented magnetic moments in the sample. This unaccounted opposite diamagnetic response leads to a dilution of the desired ferromagnetic signal of the measured thin-film. Nonetheless, diamagnetic response signal should show linear magnetic field dependence and can be therefore subtracted in order to obtain the purely ferromagnetic signal from the thin-film sample measurement.

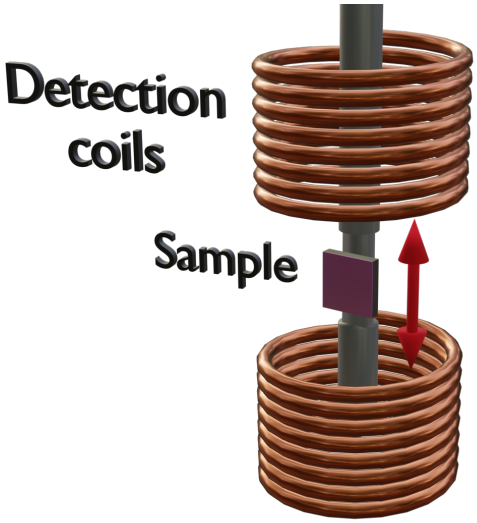

Figure 5.2: VSM measuring apparatus consists of detection coils and a sample holder, onto which a sample is placed. Vibrating sample holder forces the sample into a oscillating motion along the axis of the detection coils. Magnetic moment of the sample induces electromotive force in the detection coils. Signal recorded is thus proportional to the magnetization of the sample.

5.3. Optical microscopy

For further sample characterization an optical microscope was used. Observation of FeRh films with a wide-field microscope allows following the reflectivity changes occurring across the AF-FM phase transition, where reflectivity decreases (by about 3 %) upon heating of the sample.

Samples were characterized by using Peltier module in combination with an optical microscope with a suitable magnification (using objective lenses with 20x or 50x magnification), see Figure 5.3. Peltier heater stage was used to globally induce AF-FM or FM-AF phase transition by heating and cooling down the sample respectively. Transition was then observed by using optical microscope.

In contrast to VSM characterization method, mentioned optical setup enables us to observe magnetostructural phase transition locally, in a spatial-dependent fashion. This

method does not introduces inconsistencies caused by the substrate of the thin-film sample. In addition, using optical setup facilitates a study of the domain nucleation and growth, as will be demonstrated in the following chapter.

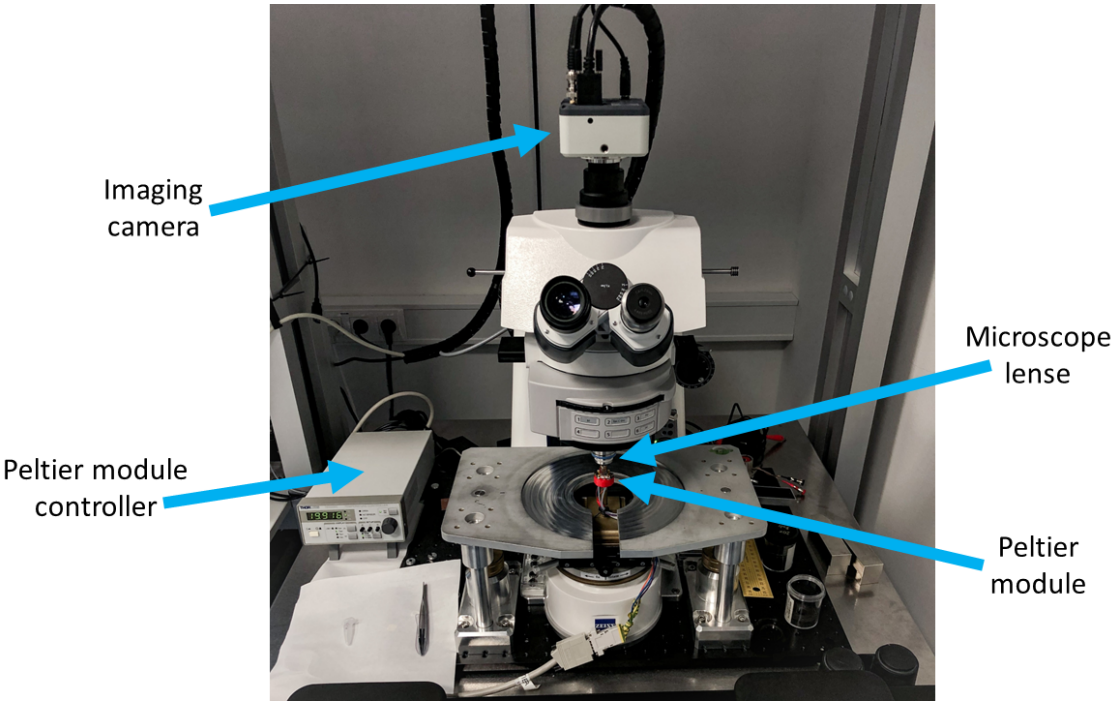

Figure 5.3: Optical microscope setup consisting of Peltier heater stage, suitable magnification lens and CCD camera. The Peltier heater stage was controlled using a custom-made software that allows setting a target temperature. The temperature controller adjusts the magnitude of the bipolar current in the Peltier module using a proportional–integral–derivative (PID) controller.

5.4. Ultrafast laser setup

For purposes of our laser induced magnetic phase transition experiments a Coherent Monaco 1035-40 pump laser source was used [24]. A parametric amplifier Opera-F and a pulse compressor was then used to transform initial pulses with wavelength $\lambda = 1035$ nm and temporal pulse width $t_w < 350$ fs into more suitable pulses with wavelength $\lambda = 805$ nm and $t_w < 40$ fs. The power output is dependent on repetition rate, for used pulses with repetition rate of 20 kHz an output of 25 mW was measured, which is equivalent to an energy of 1.25 μJ per pulse.

As seen on the scheme of the laser setup 5.4, laser pulse is being split by a beam-splitter (BS), although for the current laser experiments only reflected beam is used, however this particular optical path design is envisioned for future pump-probe experiments that enable time-resolved characterization. Reflected beam is then directed through a delay stage towards a nonlinear crystal where second-harmonic-generation occurs (SHG). SHG generates pulses with half the wavelength of initial pulses (pulses with a central wavelength of 400 nm are being generated). Harmonic beam-splitter (HBS) is then being used to separate light with with the remaining 800 nm light after nonlinear crystal (as conversion

is not 100 % efficient), which is then caught by the beam-blocker. The transmitted 400 nm light pulses are sent to a linear polarizer (P) and subsequently to a quarter waveplate (R). Finally, light is focused onto the sample using a biconvex lens (L) with a focal length of 200 m. By selecting the appropriate relative orientation of the polarizer P and waveplate R, one can select a desired polarization state of light between right circularly polarized (RCP), left circularly polarized (LCP) or linear polarized (LIN), that will be used to pump the sample. This is achieved by precisely rotating querter-wave plate via Thorlabs motorized rotation mount K10CR1/M. Laser setup was build, aligned and tested in collaboration with my colleague Jakub Opršal.

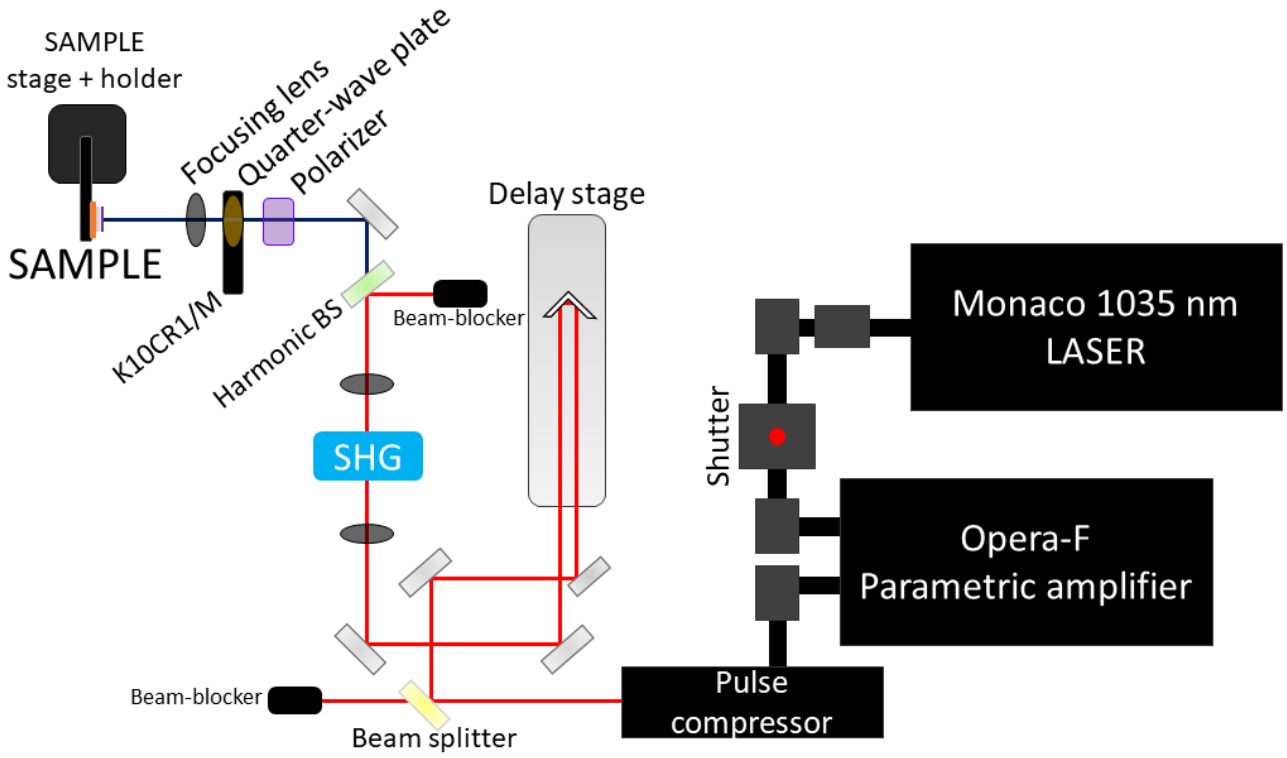

Figure 5.4: Figure shows a schematic of femtosecond laser based optical setup for laser-induced control of magnetic phase transitions. Ultrashort laser pulses with a wavelength of 800 nm are directed to a nonlinear crystal in order to convert light to 400 nm via second harmonic generation (SHG). The polarization state of the light pulses incident on the sample can be selected by the combination of different optics (P - polarizer, R - quarter waveplate). The light is then focused on the sample using a lens (L). The sample position can be manipulated using stepper motors that allow motion in the three dimensions, enabling laser sweeping experiments.

6. Phase transition characterization of FeRh thin films

The present chapter describes preparation of suitable samples for later experiments, as well as the characterization process and results. Samples were prepared using processes and tuning techniques described in Section 4.2. In order to distinguish suitable samples, characterization process was carried out using VSM and optical microscope set-up. It is also shown that the analysis of optical microscopy images for different temperatures allows evaluating the phase transition characteristics without the need of performing magnetic measurements.

6.1. Growth of thin-film FeRh samples

One of the planned tasks of this thesis was to prepare suitable FeRh film samples on single-crystal oxide substrates via magnetron sputtering. In this work, samples of thin-film FeRh were grown using magnetron sputtering onto a single-crystal oxide substrates. Sputtering process commenced by introducing a suitable substrate into a chamber with base pressure lower than 5×10^{-8} mbar . The substrates were preheated to 623 K for 1h prior to the deposition process and FeRh was then grown at the same temperature using a equiatomic FeRh target.

In order to perform later experiments successfully and consistently at room temperature, it is vital that prepared samples exhibit magnetostructural phase transition approximately room temperature $T = 300$ K. More importantly, suitable sample must ideally have the FM-AF transition temperature below room temperature. Meaning, correctly prepared sample must retain FM domains at room temperature.

This property is accomplished using various transition temperature tuning methods as described in chapter 4.2. Three FeRh films were utilized, each with a different temperature tuning approach, shown on figure 6.1.

Sample I - tuning by altering FeRh composition

Sample I was deposited at Ar atmosphere with pressure 2.6×10^{-3} mbar onto a $MgO(001)$ substrate, using sputter power of 50 W. Obtaining 40 nm thick slightly iron rich thin-film sample ($Fe_{1-x}Rh_x$ for $0.48 \leqslant x < 0.50$) with a FeRh(001) out-of-plane crystallographic texture.

Sample II - tuning by tensile in-plane stress

Thin film FeRh sample with 50:50 alloy composition was obtained at Arg pressure 2.8×10^{-3} mbar . Using a sputter power of 50 W yielded deposition rate of 0.03 nm/s. Thin-film was grown on $Al_2O_3(0001)$ substrate which induced tensile in-plane stress, as described in chapter 4.2 . Resulting 25 nm thick FeRh layer had a FeRh(111) out-of-plane crystallographic texture.

Sample P52b (III) - tuning by carbon doping

Deposition of sample III was done at Ar pressure of 2.8×10^{-3} mbar onto a $MgO(001)$ substrate. Using simultaneous confocal sputtering of FeRh and C targets, carbon was introduced into the thin film of FeRh. Sputtering power and corresponding material deposition rates were carefully adjusted, in order to achieve $(FeRh)_{96}C_4$ composition. Similarly to sample I the resulting thickness was 40 nm with a FeRh(001) out-of-plane crystallographic texture.

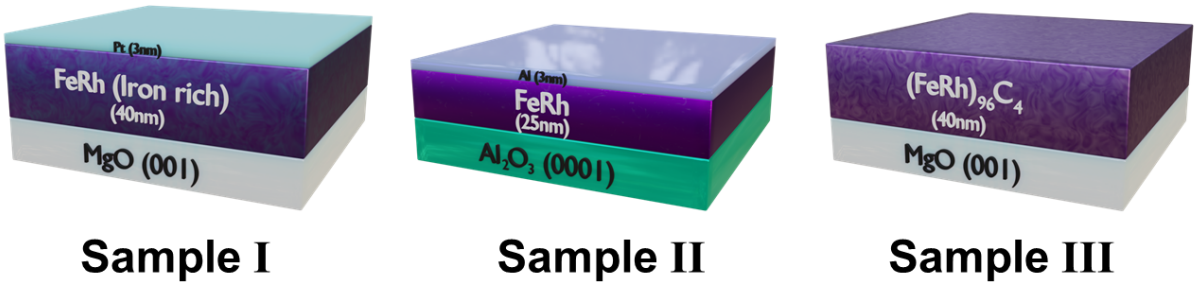

Figure 6.1: Samples I, II, III were prepared using three different methods of transition temperature tuning. sample I posses a FeRh composition with slightly higher iron value ($Fe_{1-x}Rh_x$ for $0.48 \leqslant x < 0.50$). Sample II uses $Al_2O_3(0001)$ as a substrate which induces tensile in-plane stress. For sample III, FeRh layer was doped with carbon ($(FeRh)_{96}C_4$)

In 1968 R. C. Wayne[25] described the effect of thermal treatment on FeRh phase transition. He concluded that cooling process strongly impacts the behavior of the phase transition. Later in 1999, J. van Driel [26] described the annealing process significance when concerned with layer transformation to the CsCl-type crystal structure.

All of the prepared samples were thus post-growth annealed at 923 K for 45 min to obtain desired CsCl-type crystal structure. Samples I and II were subsequently cooled down below 375 K and capped with a 3-nm-thick Pt or Al antioxidation protective layer. Sample III was left uncapped.

6.2. Magnetization characterization

For purposes of deeper understanding of the sample behavior, a more complex characterization was needed. Vibrating sample magnetometry was used to measure sample magnetization dependence on external magnetic field. Perhaps more importantly, sample magnetization dependacnce on temperature was later also measured, in attempt to detect both AF-FM and FM-AF phase transition. Sample characterization is vital for determination whether or not the samples are suitable for later experiments.

6.2.1. Field hysteresis

The three FeRh film samples were initially characterized at 400 K by measuring the magnetization dependence on magnetic field in the range between -1 T and 1 T. The

resulting field hysteresis curves are shown in Figure 6.2. Resulting field driven hysteresis curves were recorded, as shown in figure 6.2.

In addition, field hysteresis loops were also measured at temperatures below room temperature (200 K or 250 K). The low temperature measured loops are shown together with the hysteresis curves measured at 400 K. For all samples, we observe a noticeable change of the magnetization when going from 400 K to low temperature (200 K or 250 K), which is a fingerprint of the FM-AF phase transition.

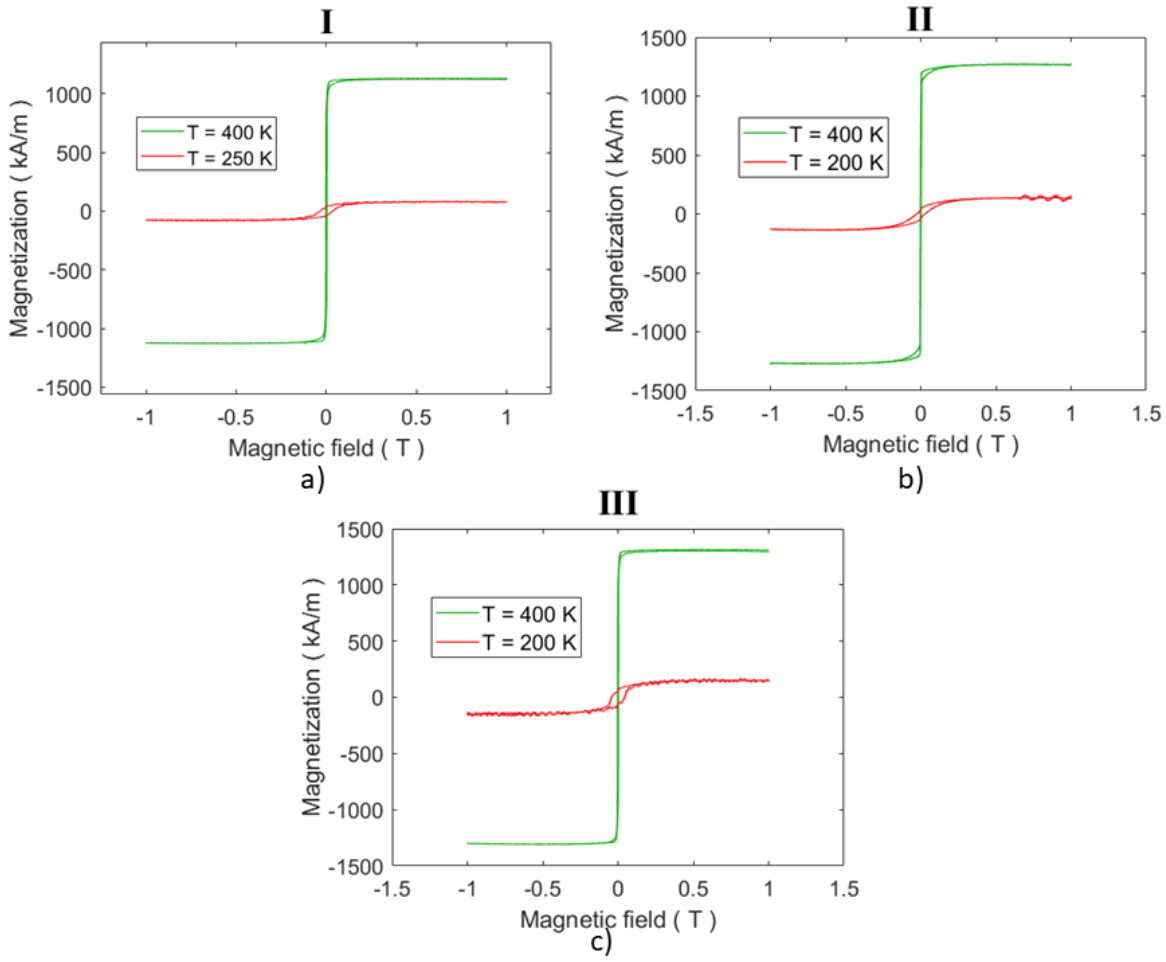

Figure 6.2: Combination of hysteresis recorded at high temperature (400 K) and hysteresis recorded at low temperature (200 K or 250 K)

.

It is also worth commenting on the non-zero magnetization saturation value at low temperatures. The sample is expected to be in a fully antiferromagnetic state at these temperature ($T \sim 200$ K shown on Figure. 6.3), thus should be exhibiting zero magnetic moment (no FM domains should be present). Recorded non-zero magnetic moment imply residual ferromagnetic domains in the now "fully" antiferromagnetic FeRh thin film. Phenomena describing this unexpected behavior was described in 2016 by F. Pressacco [11]. It was shown that these remnant ferromagnetic domains are present in top atomic layers of the sample. Unfortunately, VSM can only measure ferromagnetic signal of the full sample volume, and is therefore unable study surface specific domains.

6.2.2. Thermal hysteresis

In order to further understand the magnetostructural phase transition of prepared FeRh samples, additional temperature varying characterization was performed. At constant external magnetic field H of 1 T sample was subjected to a heating process from initial temperature $T = 200\,\mathrm{K}$ up to final temperature $T = 400\,\mathrm{K}$. Afterwards, sample was cooled back down from $T = 400\,\mathrm{K}$ to initial $T = 200\,\mathrm{K}$, and thus completing full thermally driven hysteresis curve in Figure 6.3. As previously mentioned, magnetization reaches a saturation point when sample is sufficiently heated up, concluding AF-FM phase transition and indicating a fully ferromagnetic state. When cooling, the magnetization drops to initial value, hence returning to a fully antiferromagnetic phase as a result of FM-AF phase transition. Fig. 6.3 serves as a proof that in previous measurements (displayed on fig. 6.2), samples were in a fully ferromagnetic state when a field driven hysteresis at $T = 400\,\mathrm{K}$ was recorded. Phenomenon concerning non-zero remnant magnetization is likewise present.

Main focus of aforementioned experiments is to record the phase transition temperatures. Observations of phase transition temperature is vital for determination whether given sample is suitable for later experiments. Transition temperatures are required to be approximately $T = 300\,\mathrm{K}$, more importantly it is essential that FM-AF phase transition temperature is lower than room temperature. Full reasoning behind this requirement will be clarified in later experimental chapter. Either transition temperature is defined as the steepest slope of each transition, in other words, the point (transition temperature value) in which first order derivation returns a discontinuity. These recorded values of both AF-FM and FM-AF transition temperatures are recorded in table 6.1

Following three graphs depict temperature characterization corresponding to each of the samples 6.3. Since transition temperatures of each sample are approximately $T = 300\,\mathrm{K}$, we conclude prepared samples to be suitable for later experiments. Using VSM, temperature characterization grants more precise understanding of *when* the magnetostructural phase transition takes place.

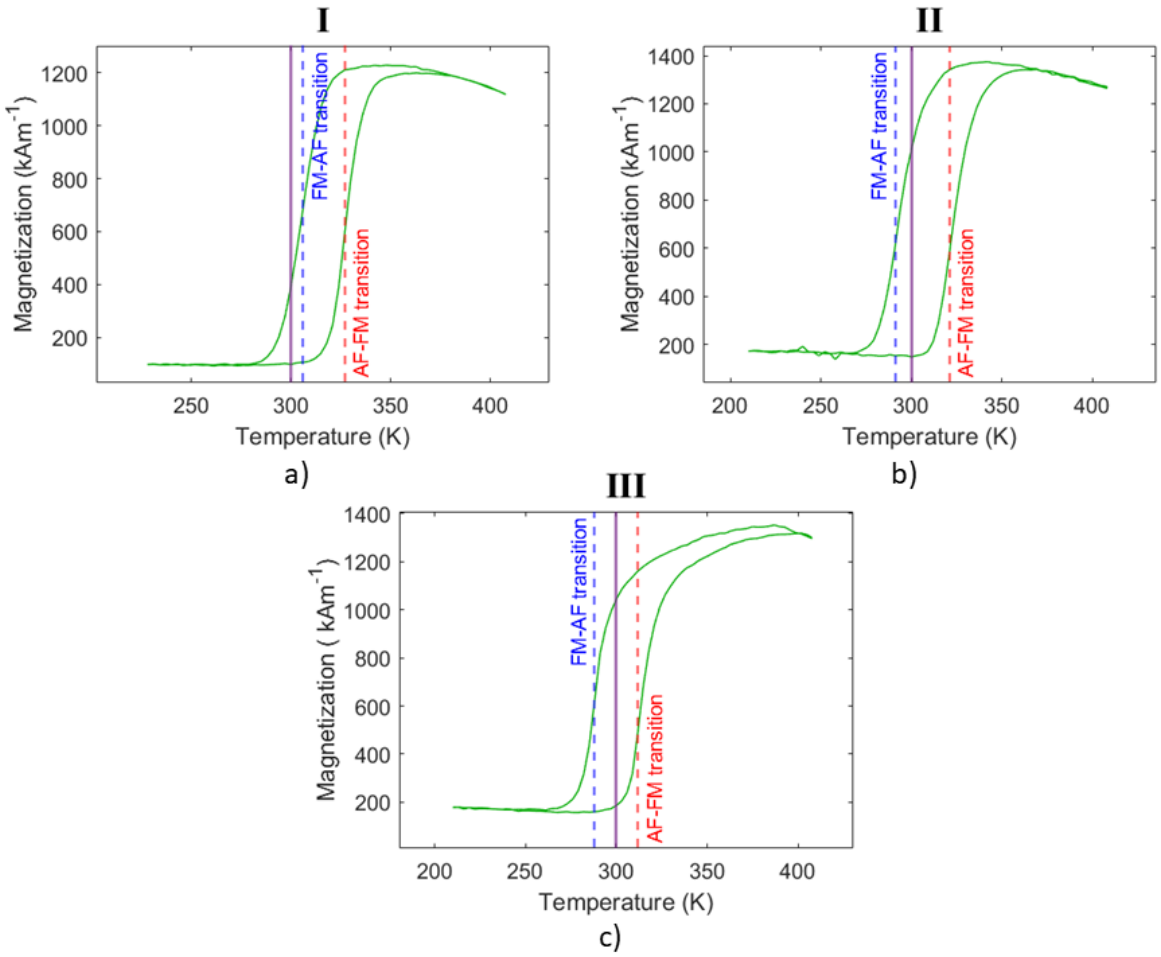

Figure 6.3: graphs show temperature dependence of magnetization of FeRh films. Dotted lines symbolize AF-FM and FM-AF phase transitions. Transition temperatures are compared to solid purple line, symbolizing temperature value of 300 K.

	I	II	III
M_S FM phase (kA/m)	1129	1275	1318
M_S AF phase (kA/m)	81	139	153
H_C FM phase (mT)	1.6	1.1	1.4
H_C AF phase (mT)	32	29	44
Residual FM magnetization (%)	6.8	10.9	11.6
AF-FM transition (K)	326.9	321.0	311.8
FM-AF transition (K)	306.0	291.0	288.0
Width of hysteresis (K)	20.9	30	23.8

Table 6.1: Table containing characteristic values of samples I, II and III

6.3. Optical characterization

VSM proved to be greatly useful tool for sample characterization, however it lacks a region specific description of phase transitions. All previously recorded data were describing

phase transition process for the bulk of the sample. More precise local observation of phase transition (domain growth on the surface of the sample) could be insightful. During magnetostructural phase transition a reflectivity change takes place [16]. Essentially meaning that, FM and AF domains do exhibit different reflectivity values (around 3 % change occurs). One can utilize this important difference between AF and FM domains with an optical microscope. Thus observing a lighter (higher reflectivity regions) and darker (lower reflectivity regions) parts of the sample. During this characterization, a sample was being heated using a Peltier module setup in combination with an optical microscope. Peltier module heated globally the bulk of a sample, similarly to VSM. However, using optical microscope a domain growth on the surface of the sample has been observed. Samples were being heated in small temperature adjustments ($\delta T = 2\,\mathrm{K}$ for temperature region outside of the transition and $\delta T = 1\,\mathrm{K}$ during the phase transition) from a fully AF phase through a AF-FM phase transition towards a fully ferromagnetic phase. For every temperature adjustment a microscope image was taken. During heating through a AF-FM phase transition threshold, utilizing suitable magnification lens (magnification 20x and 50x was being used depending on the amount of detail required) growth of dark spots (ferromagnetic domains) was recognized as shown in figure 6.4. The growth continued until the samples appeared to be completely dark due to now lowered reflectivity, indicating a fully ferromagnetic state. Once fully FM phase was reached, using Peltier module a sample cooling process was initiated. Similarly to previous heating process, cooling was done in small temperature adjustments from fully FM phase towards fully AF phase. Difference being, when crossing the FM-AF transition temperature, light spots started to appear and grow throughout the sample surface. Light spots represent regions with lower reflectivity, recognized as AF domains. Once the sample is back in initial fully antiferromagnetic state, sample appears completely light. Images obtained using optical microscope were then analyzed. Custom code for gray-scale value recognition was made, including defect exclusion and region specific targeting. Gray-scale values represent specific reflectivity values of the sample. Processing images (images taken throughout the heating and cooling of the sample) using this code, region specific hysteresis of gray-scale (reflectivity) value versus temperature was obtained. This enabled a region specific study of transitions on the sample surface.

In contrast to previous VSM characterization, using which understanding of *when* magnetostrucutral phase transition takes place was gained, using optical microscopy for characterization provided insight to *how* magnetostrucutral phase transition takes place.

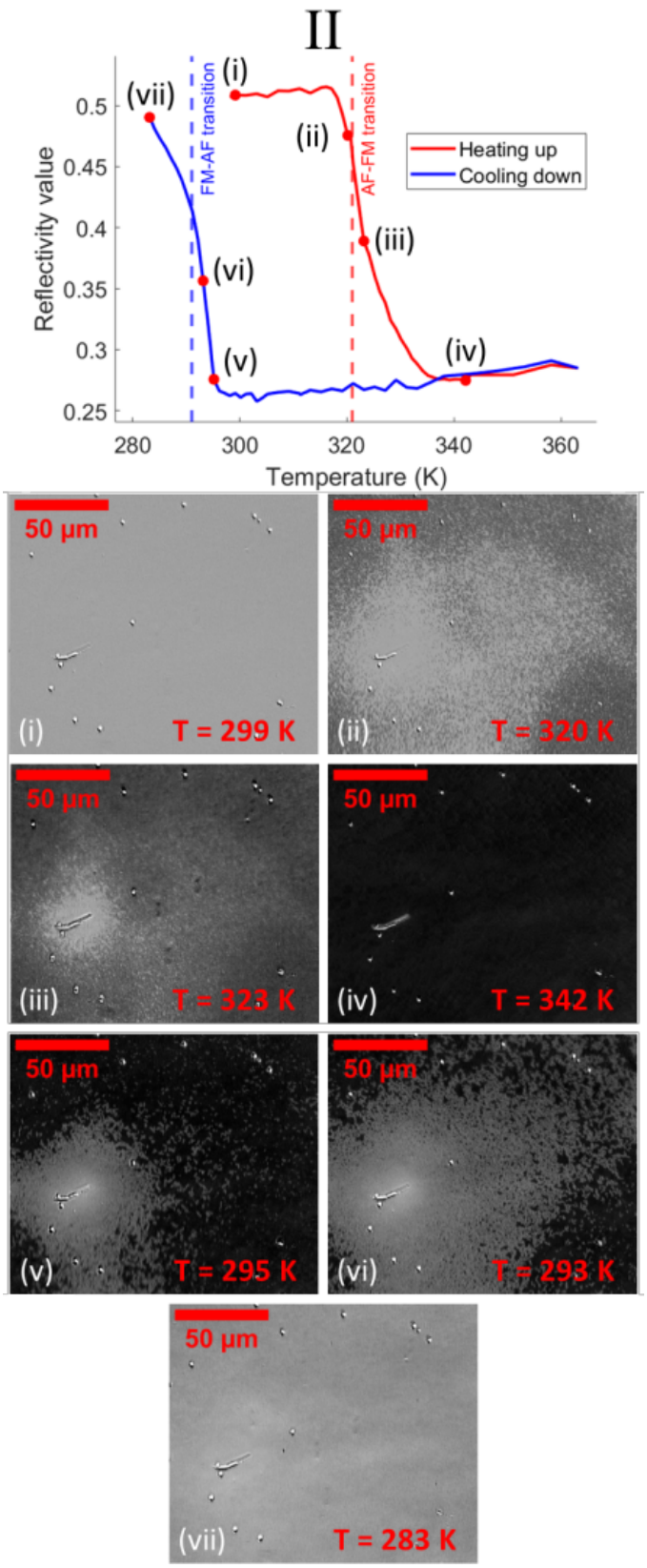

(a)

Figure 6.4: Using a custom developed code, reflectivity values (represented by grayscale values) of surface of the sample were recorded throughout the heating and cooling of the sample. Resulting images show growth of FM domains and subsequently AF domain when sample is being cooled down.

7. Laser-induced magnetization writing in FeRh

In order to show the selective laser-induced writing of FM domains in an FeRh thin film, we selected the Sample II (25 nm FeRh on Al_2O_3), which fulfills the condition of bistable AF and FM phases around room temperature.

7.1. Irradiation of FeRh

As mentioned in chapter 5.4 laser set-up was build 5.4. Sample was placed onto a sample stage, which consisted of sample holder and linear motors. Computer controlled motors enabled us to move sample in three directions with varying speeds of movement. Using a focusing lens (L), laser pulses were focused onto the sample holder. Furthermore, samples was placed under a 10 degree angle on vertical axis, making blocking of reflected pulses simpler and preventing back-scatter. However this slight tilt in relation to incident laser pulses means that when sample is being shifted, incident laser pulses are marginally out of focus when making contact with sample surface

Quarter-wave plate was mounted on a Thorlabs motorized rotation mount K10CR1/M. This enabled adjustment of angle of quarter-wave plate in correlation to the rotation angle of polarizer to be precisely adjusted. Using this setup granted generation of right-circularly polarized (RCP), left-circularly polarized (LCP) and linearly polarized light (LIN).

FeRh sample was initially cooled down to $T = 200\,\mathrm{K}$ utilizing VSM. This was done to assure a fully antiferromagnetic state of the sample. At the sample holder laser beam with pulse repetition of 20 kHz was measured to have power of 1.2 mW. Such power yields single pulse energy of 60 nJ . Samples were attached in such a way, that laser beam was initially not hitting the sample. Using motors to control the sample stage, sample was shifted in order to make the laser beam sweep through the sample surface in a 'S' shaped manner as shown on the top of figure 7.1. The speed of laser beam sweep was set to 0.1 mm/s. Initial laser beam sweep path (top one, left to right) possessed a LCP and was swept horizontally. Sample was then moved in order to drop the laser beam lower (middle position), where the polarization was switched to RCP. Beam was then swept horizontally (right to left) and then vertically dropped once more (bottom lane). Polarization was subsequently switched to LIN before laser was swept. Beam was then blocked off, creating a sharp end of the path. Once the sample was irradiated it was moved to optical microscope for analysis. As mentioned in previous chapter, AF and FM regions will have different reflectivity values. Optical microscope thus provides ability to differentiate regions where laser induced magnetostructural phase transition (AF-FM phase transition). Contrast of images taken on the optical microscope was enhanced by taking a background image of the area where laser was swept and slightly offsetting the actual image. For certain areas, enhancing the contrast of the images was sufficient. Images 7.1 correspond exactly to the path where laser beam was swept. Thus proving that laser induced magnetization on FeRh film took place. Laser beam path images also show that some regions, where laser was swept, did not fully undergo AF-FM phase transition. This can be caused by the insufficient energy of a single pulse.

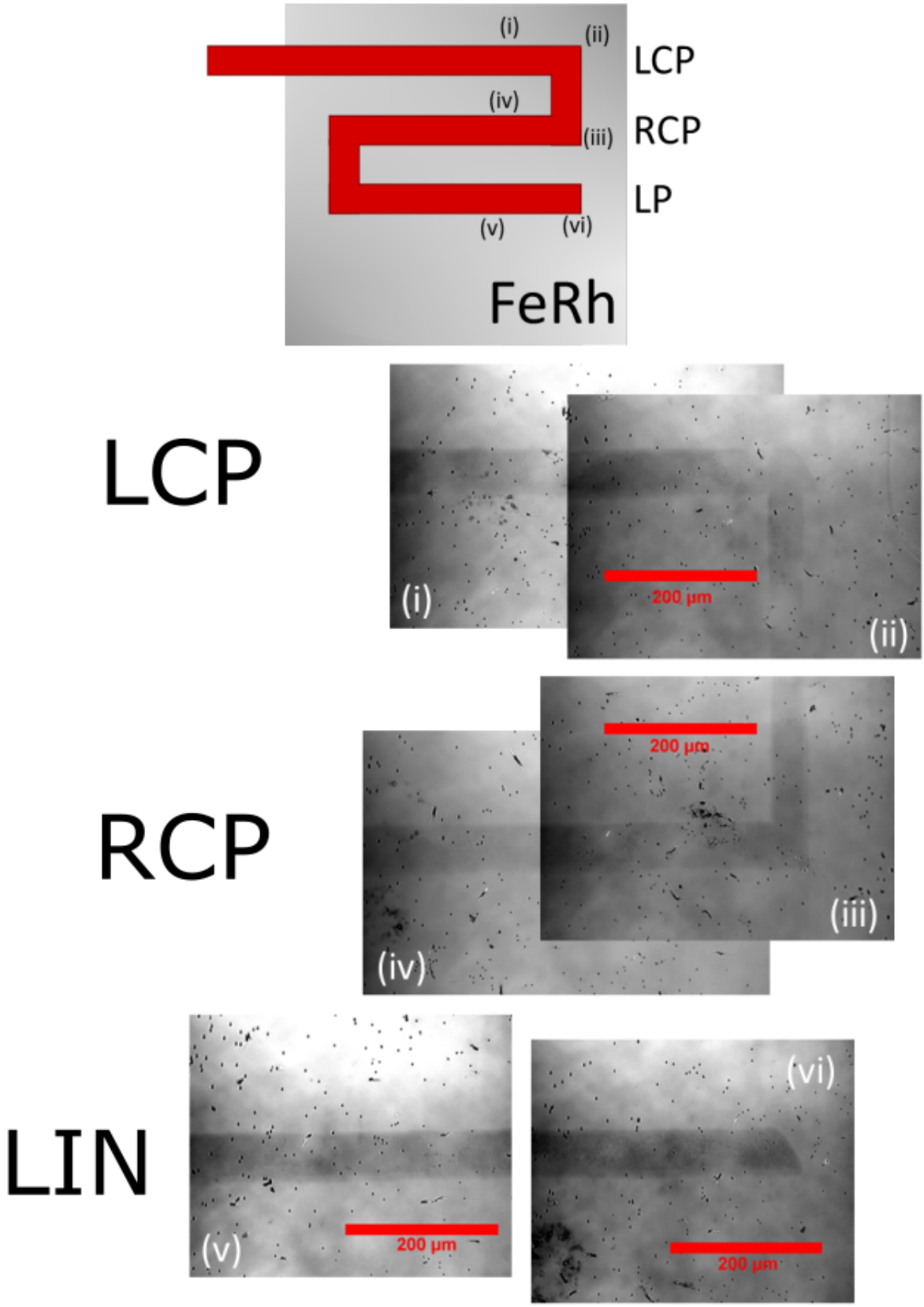

Figure 7.1: Sweeping path of the laser beam across the sample is shown in the top part of the figure. Images underneath were produced using optical microscope with 20x magnification lens. Image collage accurately corresponds to the beam path of the laser.

Hypothesis

For better contrast of the irradiated area, a background image was took and actual image was then shifted to gain a slight offset. Such method was used on Figure 7.3. It shows the end of the sweeping path of the laser beam. When enhanced using a mentioned method, areas of different grayscale values (different reflectivity values) are apparent in the line region where laser was swept. Although the line region is ferromagnetic, some regions appear to be darker. This interesting result may point to laser induced depth magnetization. The laser pulses are of Gaussian character and thus posses the highest power output in the center of the beam. It is thus possible, that the power increase in the center may have induced magnetization deeper into the sample. Where edges of the beam were only able to induce magnetization on the surface of the FeRh film. Higher depth of ferromagnetic domains consequently appears as darker spots within the laser beam footprint.

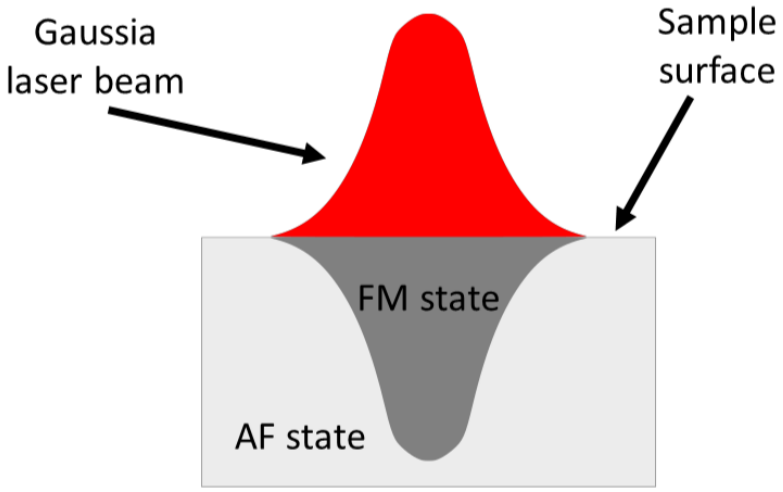

Figure 7.2: Hypothesized affect of Gaussian beam footprint on sample volume.

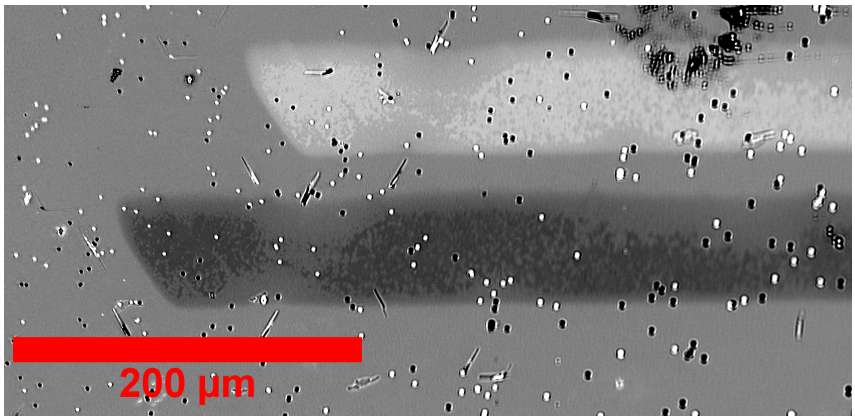

Figure 7.3: FeRh film irradiated by linearly polarized light. Figure was produced by offseting image from background image. Different darkness levels (possibly different FM depths) are visible on the edges of the laser beam path.

Conclusion

Ever increasing computation speeds of modern processors demand equivalently rapid way of writing and storing data. In attempt to perform such ultrafast storage of data based on magnetic materials, a new way of sub-picosecond magnetization was researched. Past few decades of research have shown, that ultrafast laser induced magnetization is a promising option.

Thesis introduced the concept of ultrafast laser induced magnetization and offered possible approach of performing this experiment. In theorerical part of the thesis, FeRh was later suggested as convenient material which is capable of performing laser induced magentization. Preparations for this experiment consisted of sample growth using physical vapor deposition method of magnetron sputtering and subsequent sample characterization. Suitable sample was required to be able to sustain laser induced ferromagnetic domains for long periods of time at room temperature. Such samples were prepared by employing transition temperature tuning techniques. Three samples were prepared, each with different concept of temperature tuning. Sample I was tuned via composition alteration ($Fe_{1-x}Rh_x$). Sample II was deposition onto a sapphire substrate induced tensile in-plane stress, which consequently altered phase transition temperature. By doping FeRh film of sample III, the phase transition temperature was also tuned to be more suitable for laser experiment. Attained samples were consequently characterized by using vibrating sample magnetometry and optical microscopy. Vibrating sample magnetometry granted a way of recording field driven and more importantly thermally driven hysteresis curves. Measurements yielded precise values of phase transition temperatures for antiferromagnetic-to-ferromagnetic and ferromagnetic-to-antiferromagnetic were determined for samples I, II, and III to be 325.9 K and 306 K, 321 K and 291 K, and 311.8 K and 288 K, respectively. Characteristic values of magnetization saturation, coercive field, residual magnetization and temperature difference between phase transition temperatures were extracted from the magnetometry data. In addition to film-integrated characterization of samples, optical microscopy served as essential tool for the study of the spatial-resolved, local domain nucleation and growth study. Custom code in combination with microscopy images offered an insightful information on surface region specific domain growth. Combining results of both methods granted a deeper understanding of *how* and *when* aforementioned magnetostructural phase transition takes affect. Characterization yielded a positive outcome and thus deeming samples suitable for laser experiment. For the final experiment of laser induced magnetization, a custom laser set-up was build. Ultrashort laser pulses originated from a Monaco 1035 pulsing laser, passed through a Opera-F parametric amplifier and were guided through second harmonic generation towards polarizer, quarter wave-plate, lens set-up where polarization switching was performed. Laser beam was then swept through the surface of the sample using motorized sample stage and three different polarizations. Subsequent observation of irradiated FeRh thin film using optical microscopy showed stable ferromagnetic domains in a laser path pattern. Thus concluding the experiment and proving that FeRh thin films were prepared correctly. In combination with characterization by magnetometry as a function of temperature, work performed led to a successful ultrafast laser induced magnetization.

Future development of this experiment is based on performing time resolved ultrafast laser induced magnetization. This pump-probe experiment will grant the possibility of studying time frames at which ultrafast magnetization arises.

Bibliography

[1] E. Beaurepaire, J.-C. Merle, A. Daunois, and J.-Y. Bigot, *Ultrafast spin dynamics in ferromagnetic nickel*. Phys. Rev. Lett. 76, 4250–4253 (1996).

[2] M. Mansuripur,*Physical Principles of Magneto-Optical Recording* (Cambridge University Press, Cambridge, England, 1998).

[3] C. H. Back *et al.*, *Minimum field strength in precessional magnetization reversal*. Science 285, 864-867 (1999).

[4] I. Tudosa *et al.*, *The ultimate speed of magnetic switching in granular recording media*. Nature 428, 831-833 (2004).

[5] C. Stanci *et al.*, *All-Optical Magnetic Recording with Circularly Polarized Light*. Physical Review Letters 99, 047601 (2007).

[6] A. V. Kimel *et al.*, *Ultrafast non-thermal control of magnetization by instantaneous photomagnetic pulses*. Nature 435, 655-657 (2005).

[7] A. Kirilyuk, A. V. Kimel,and T. Rasing, *Ultrafast optical manipulation of magnetic order*. Review of Modern Physics 82, 2731–2784 (2010).

[8] J. Coey, *Magnetism and Magnetic Materials* (Cambridge: Cambridge University Press, 2010).

[9] S. Blundell, *Magnetism in condensed matter* (Oxford, Oxford University Press, 2001).

[10] J. Stöhr, and H.C. Siegmann, *Magnetism: From Fundamentals to Nanoscale Dynamics* (Springer, 2006).

[11] F. Pressacco *et al.*, *Stable room-temperature ferromagnetic phase at the FeRh(100) surface*. Scientific Reports 6, 22383 (2016).

[12] H. Nishimori, and G. Ortiz, *Elements of Phase Transitions and Critical Phenomena*)(Oxford, Oxford University Press, 2010).

[13] M. Fallot, and R. Hocart, *Sur l'apparition du ferromagnétisme par élévation de température dans des alliages de fer et de rhodium*. Revue Scientifique 77, 498-499 (1939).

[14] L. H. Lewis, C. H. Marrows, and S. Langridge, *Coupled magnetic, structural, and electronic phase transitions in FeRh*. Journal of Physics D: Applied Physics 49, 323002 (2016).

[15] L. J. Swartzendruber,*The Fe-Rh (Iron-Rhodium) System*, Bulletin of Alloy Phase Diagrams 5, 456–462 (1984).

[16] V. Saidl *et al.*, *Investigation of magneto-structural phase transition in FeRh by reflectivity and transmittance measurements in visible and near-infrared spectral region*. New Journal of Physics 18, 083017 (2016).

[17] S. Maat, J.-U. Thiele, and E.E. Fullerton, *Temperature and field hysteresis of the antiferromagnetic-to-ferromagnetic phase transition in epitaxial FeRh films*. Physical Review B 72, 214432 (2005).

[18] G. Shirane, R. Nathans, and C. W. Chen,*Magnetic Moments and Unpaired Spin Densities in the Fe-Rh Alloys*. Physical Review 134, A1547–A1553 (1964).

[19] M. Rosenberg *et al.*, *A Mössbauer spectroscopy and magnetic study of FeRh*. Journal of Magnetism and Magnetic Materials 177, 135-136 (1998).

[20] J. S. Kouvel, *Unusual Nature of the Abrupt Magnetic Transition in FeRh and Its Pseudobinary Variants*. Journal of Applied Physics 37, 1257–1258 (1966).

[21] R. Barua, F. Jiménez-Villacorta, and L. H. Lewis, *Predicting magnetostructural trends in FeRh-based ternary systems*. Applied Physics Letters 103, 102407 (2013).

[22] A. I. Zakharov *et al.*, *Magnetic and magnetoelastic properties of a metamagnetic iron-rhodium alloy*. Soviet Physics JETP 19, 1348-1353 (1964).

[23] H. H. Gatzen, V. Saile, and J. Leuthold, *Micro and Nano Fabrication* (Springer, 2014).

[24] In depth description of laser source Monaco 1035 can be found on manufacturers website, Coherent, https://www.coherent.com/lasers/ultrashort-pulse/monaco

[25] R.C. Wayne, *Pressure Dependence of the Magnetic Transitions in Fe-Rh Alloys*. Physical Review 170, 523–527 (1968).

[26] J. van Driel *et al.*, *Compositional dependence of the giant magnetoresistance in F exRh1−x thin films*. Journal of Applied Physics 85, 1026–1036 (1999).

Appendix

Additional sample preparation

One of the main goals of this thesis was sample preparation. Due to the expensive nature of FeRh alloy, Most of my sample preparation processes were dedicated to growth of CoGd and CoPt single and multi-layer samples. Already existing samples of FeRh (I,II,III) were prepared by Jon Ander Arregi. CoGd and CoPt single and multi-layer samples were then used for laser irradiation experiments by my colleague Jakub Opršal. This served as a direct familiarizing process with magnetron sputtering and general sample preparation processes. Samples prepared for Jakub Opršal are listed in tables below.

	Thickness of Co (nm)	
Repetitions	0.4	0.6
1x	[Co(0.4)/Pt(0.7)]	[Co(0.6)/Pt(0.7)]
3x	$[Pt(0.4)/Pt(0.7)]_3$	$[Pt(0.6)/Pt(0.7)]_3$
8x	$[Pt(0.4)/Pt(0.7)]_8$	

Table 7.1: Summary of all used Co/Pt samples. Substrate used for all mentioned samples was Si wafer with native oxide on the surface. All samples were the capped with 3 nm Pt layer.

	Thickness of Co (nm)		
Repetitions	1.0	1.2	1.4
1x	Co(1)/Gd(3)	Co(1.2)/Gd(3)	Co(1.4)/Gd(3)

Table 7.2: Summary of all used Co/Gd samples. Substrate used for all mentioned samples was Si wafer with native oxide on the surface. All samples were the capped with 3 nm Pt layer.